



HAL
open science

Structure and Collision-Induced Dissociation of the protonated cyclo His-Phe Dipeptide: Mechanistic Studies and Stereochemical Effects

Ariel Pérez-Mellor, Katia Le Barbu-Debus, Valeria Lepere, Ivan Alata, Riccardo Spezia, Anne Zehnacker

► **To cite this version:**

Ariel Pérez-Mellor, Katia Le Barbu-Debus, Valeria Lepere, Ivan Alata, Riccardo Spezia, et al.. Structure and Collision-Induced Dissociation of the protonated cyclo His-Phe Dipeptide: Mechanistic Studies and Stereochemical Effects. *The European Physical Journal D: Atomic, molecular, optical and plasma physics*, 2021, 75 (6), 10.1140/epjd/s10053-021-00173-w . hal-03249830

HAL Id: hal-03249830

<https://hal.science/hal-03249830v1>

Submitted on 4 Jun 2021

HAL is a multi-disciplinary open access archive for the deposit and dissemination of scientific research documents, whether they are published or not. The documents may come from teaching and research institutions in France or abroad, or from public or private research centers.

L'archive ouverte pluridisciplinaire **HAL**, est destinée au dépôt et à la diffusion de documents scientifiques de niveau recherche, publiés ou non, émanant des établissements d'enseignement et de recherche français ou étrangers, des laboratoires publics ou privés.

Structure and Collision-Induced Dissociation of the protonated cyclo His-Phe Dipeptide: Mechanistic Studies and Stereochemical Effects.

Ariel Pérez-Mellor,^{a)b)} Katia Le Barbu-Debus,^{a)} Valeria Lepere,^{a)} Ivan Alata,^{a)} Riccardo Spezia,^{b)} Anne Zehnacker^{a)} *

a) *Université Paris-Saclay, CNRS, Institut des Sciences Moléculaires d'Orsay, 91405, Orsay, France*

b) *Laboratoire de Chimie Théorique, Sorbonne Université, UMR 7616 CNRS, 4, Place Jussieu, 75005 Paris, France.*

* anne.zehnacker-rentien@universite-paris-saclay.fr

Abstract

The role of stereochemical factors on the structure and the fragmentation paths of the protonated cyclic dipeptide cyclo histidine-phenylalanine is studied under ion traps conditions by combining tandem mass spectrometry, laser spectroscopy, quantum chemical calculations and chemical dynamics simulations. Vibrational spectroscopy obtained by Infrared Multiple Photon Dissociation (IRMPD) reveals a small difference between the two diastereomers, c-LLH⁺, and c-LDH⁺, arising mainly from ancillary CH... π interactions. In contrast, there is a strong influence of the residues chirality on the collision-induced dissociation (CID) processes. Chemical dynamics simulations rationalize this effect, and evidence that proton mobility takes place, allowing isomerization to intermediate cyclic structures that are different for c-LLH⁺ and c-LDH⁺, resulting in different barriers to proton mobility. This effect is related to the protonation of the imidazole ring. It contrasts with the minute stereochemical effects observed for other cyclic dipeptides in which the proton is borne by an amide CO.

Keywords Mass spectrometry – Collision-induced dissociation – Laser spectroscopy – IRMPD – DKP Peptides – Molecular Dynamics – Chirality

Introduction

Analytical techniques like chiral-phase chromatography have proven to be an efficient tool in separating and analyzing chiral molecules.¹ However, they do not provide direct information on the molecular structure or the interactions at play in the separation process. Coupled with electrospray ionization (ESI) or Matrix-Assisted Laser Desorption Ionization (MALDI) sources, mass spectrometry (MS) allows characterizing complex biomolecules. Combined with ion activation techniques, it provides in particular ample sequence information on peptides.²⁻⁶ A challenging aspect of MS is that it is blind to chirality. Enantiomers or diastereomers cannot be distinguished by sole single-stage MS, due to their identical masses. Separation of diastereomers by ion mobility prior to MS analysis has been proposed, for example, for alanine polymers, and evidences that changing the absolute configuration of a single amino acid disrupts its regular helical shape.⁷ Combination of cationization, multimer ions formation, and traveling wave ion mobility has been applied to the separation of diastereomers.⁸ Information can also be gained from multistage mass spectrometry MSⁿ, resorting to activation methods like electron-capture dissociation (ECD), applicable to multiply charged cations, or collision-induced dissociation (CID), applicable to a wider range of charged species, in particular peptides.⁹⁻¹⁰ Diastereomers may show different fragmentation patterns, such as the Trp cage protein. The change in the absolute configuration of a single Tyr residue induces structural modifications that manifest themselves in its ECD pattern.¹¹ MS hyphenated with laser spectroscopy allows precise structural characterization of biomolecules under isolated conditions. This technique was recently applied in the UV and IR range to study stereochemical aspects.¹² Diastereomers of alkaloids and their dimers have been distinguished by UV-induced fragmentation.¹³⁻¹⁴ Infra-Red Multiple Photon Dissociation (IRMPD) spectroscopy is a powerful tool studying the structure of, among others, protonated peptides,¹⁵⁻¹⁹ their reaction products,²⁰⁻²¹ or their post-translational modifications.²²⁻²³ It was used to characterize the structural differences between protonated di- and tetra-phenylalanine arising from different absolute configurations of the residues and stereochemical effects in 4-hydroxyproline.²⁴⁻²⁷

A wealth of collision-induced dissociation studies has been devoted to peptide structure determination as well as the parameters that influence the dissociation efficiency.^{3-4,28} In particular, the nature of the dissociation mechanism has been debated within the frame of the mobile proton model.^{4, 9, 28-31} This model states that activation of the ion induces migration of the proton to various protonation sites prior to fragmentation. It accounts in particular for the migration of the proton from the thermodynamically most stable site to the amide NH, which weakens the amide bond and results in its fragmentation. Often, the dominant fragmentation path is cleavage at the amide bonds, yielding a series of ions designated b and y depending on which subunit bears the charge.^{9,32} Further refinement has been brought to the mobile proton model using the “pathways in competition” model.⁶ In the context of the mobile proton model, special attention has been paid to histidine-containing peptides. Due to its basic character leading to the protonation of its imidazole ring, histidine plays a peculiar role in peptide fragmentation.^{33 33-34} For example, doubly-charged peptides containing both the acidic aspartic acid residue (Asp) at the C-terminus and His at the N-terminus show enhanced backbone cleavage at the C terminal relative to peptides with no His.³⁵

Cyclic species isolated in the gas phase are exemplary systems for studying stereochemical effects on both structure and CID efficiency because of the conjunction between constraints related to the ring and those brought by stereochemical factors.^{12, 36-37} Diastereomers of protonated model systems bearing several stereogenic centers show different structures, like 1-amino-2-indanol³⁸ or 4-hydroxyproline.²⁴ Besides their pharmaceutical utility³⁹⁻⁴⁰, cyclic dipeptides built on a diketopiperazine

(DKP) ring are interesting model systems to assess the structural changes resulting from a change in the relative absolute configuration of the residues. They have been studied in the gas phase, either under supersonic conditions or as protonated species isolated in an ion trap.⁴¹⁻⁴⁸ IRMPD spectroscopy, coupled with quantum chemical calculations, indicates that the structure of protonated cyclo Phe-Phe has one of the aromatic rings folded over the DKP ring and the other extended outwards.⁴⁶ Protonated cyclo Tyr-Pro shows two conformations, with the aromatic side chain either folded over the DKP ring or extended outwards.⁴¹ In both cases, the structures are similar for the two diastereomers, which only differ in the nature or strength of ancillary intramolecular interactions.^{41, 46}

The nature of the CID products of polypeptides, namely, DKP vs. oxazolone structures, has been under debate.^{21, 49-51} While most of the b_2^+ fragments of peptides containing aliphatic residues mostly show oxazolone structure, IRMPD results indicate that peptides containing histidine show coexistence of oxazolone and diketopiperazine b_2^+ fragments.^{34, 52} No general conclusion can be drawn however, and the whole sequence plays a role in the nature of the fragment. This aspect has been recently discussed based on MS³ experiments coupled with quantum chemical calculations, which suggest the coexistence of oxazolone and lactam for the singly protonated Gln-His-Ser tripeptide, the DKP being disfavored by an additional reaction step.⁵³ The fragmentation mechanism of protonated DKP dipeptides isolated in an ion trap has been questioned too. The CID of protonated model DKPs like cyclo Gly-Gly, cyclo Ala-Ala, or cyclo Ala-Gly,^{52, 54} has been widely debated, based on the experimental evidence that protonated cyclo Ala-Ala loses CO and CO+NH₃, while protonated cyclo Gly-Gly loses 2 CO at higher energy. This was tentatively explained in terms of fragmentation from the most stable O-protonated tautomer or isomerization to the N-protonated tautomer before fragmentation.⁵⁴ Trajectories-based methods are widely used to account for CID results.⁵⁵⁻⁵⁹ Recent chemical dynamics calculations have been conducted to simulate the fragmentation of cyclic dipeptide. They rest on the development of a graph-theory based analysis of an ensemble of reactive trajectories and allow simulating the MS² spectrum observed for cyclo Gly-GlyH⁺.⁶⁰ They have also been applied to describe the dissociation of cyclo Tyr-ProH⁺.⁴¹

We report a study of the protonated DKP dipeptide cyclo His-Phe, under Fourier-transform ion cyclotron resonance (FT-ICR) conditions. The molecule under study is shown in Figure 1; the two diastereomers will be denoted in short c-LLH⁺ and c-LDH⁺. Cyclo His-Phe contains a basic residue, namely, the histidine, which is expected to be the protonation site. This contrasts with the other DKP dipeptides we have studied so far, in which the proton is borne by the amide CO. We first compare the IRMPD spectroscopy results to DFT-based calculation to determine the structure of c-LLH⁺ and c-LDH⁺ and discuss it in particular in the light of the protonation site. We then use the determined structure as a starting point for chemical dynamics simulations from which we deduce the MS² mass spectrum resulting from CID of c-LLH⁺ and c-LDH⁺. Comparison between simulated and experimental CID results will shed light on the role of the absolute configuration of the residues on the CID mechanism and efficiency.

Experimental and theoretical methods

1. Experimental methods

1.a. Collision-induced dissociation

The experiments were based on tandem mass spectrometry in a FT-ICR mass spectrometer.⁶¹ The setup involved the 7T FT-ICR hybrid mass spectrometer (Bruker, Apex Qe) equipped with an Apollo II electrospray ionization source of the SMAS (Spectrométrie de Masse, Analyse et Spectroscopie) facility at the Centre Laser Infrarouge d'Orsay (CLIO).⁶²⁻⁶³ The protonated species were generated by electrospray of the studied DKP peptide at a concentration of 50 μ M in a mixture of methanol and

water (50:50). The solution was slightly acidified by adding formic acid (concentration of $\sim 10^{-6}$ M). The dipeptides were obtained from Novopep (China) (98% purity) and used as provided. For collision-induced dissociation experiments, the ions selected in the quadrupole were accumulated for 1 second in the hexapole containing argon buffer gas. MS² spectra were obtained at different collision energy by adjusting the collision voltage, as described in the results section. Each point of the MS² spectra corresponds to a different acquisition; the experiments were repeated several times and the error on the branching ratios is less than 2%.

1.b. Spectroscopic methods

Vibrational spectra were obtained by means of Infrared Multiple Photon Dissociation (IRMPD) in the fingerprint (800-2000 cm⁻¹) and OH or NH stretch (3000-3800 cm⁻¹) regions.¹⁷ After mass-selection in the quadrupole and thermalization in the hexapole, the ions were transferred to the ICR cell, where they were irradiated. The IRMPD spectra were obtained by monitoring the Ln of the total fragmentation efficiency $\phi = -\ln(P/(F + P))$ as a function of the IR wavelength, with F and P being the sum of the fragment and parent ion abundances, respectively.

For the 800-2000 cm⁻¹ region, the CLIO free-electron laser (FEL) (25Hz repetition rate) was mildly focused by a 2000 mm Ag-protected spherical mirror to a beam diameter of ~ 1 mm at the interaction zone.⁶² The spectral bandwidth (full width at half-maximum FWHM) was about 7 cm⁻¹, with a power of 1600 to 900 mW from 800 to 2000 cm⁻¹. The wavelength was calibrated by simultaneously recording the spectrum of a polystyrene sheet. An additional broadband CO₂ laser synchronized with CLIO was used during irradiation to increase fragmentation efficiency; its pulse length was adjusted to minimize non-resonant photo-dissociation of the molecule. For the 3 μ m spectral region, an IR Optical Parametric Oscillator (LaserVision OPO, 25 Hz, 5-10 mJ/pulse) was slightly focused by the same spherical mirror.

The irradiation time was adjusted to avoid saturation of the most intense transitions, *i.e.*, to keep $\phi < 1$. In the CLIO FEL region, the irradiation time was between 250 ms and 1s, and in the OPO range, it was 2s with the CO₂ irradiation fixed at 10 ms.

2. Theoretical methods

2.a. Calculations of the stable structures

The potential energy surface (PES) was explored using the OPLS-2005 force fields with the advanced conformational search implemented in the MacroModel suite, a part of the Schrödinger package.^{64,64} The PES was explored in the gas phase, using as a starting point each possible protonation site (imidazole, oxygen and nitrogen atoms of each amide bond). All the protonated peptides structures found thereby with energy below 5 kcal/mol relative to the most stable form were optimized in the frame of the Density Functional Theory (DFT) using the dispersion-corrected functional B3LYP-D3 associated with the 6-311++G(d,p) basis set.⁶⁵⁻⁶⁷ Inclusion of empirical dispersion corrections is important for peptides with aromatic residues, in particular to account for OH... π , NH... π , and CH... π , interactions.⁶⁸⁻⁷⁰ For a more complete survey of the PES, structures were also built from the most stable neutral conformers of cyclo Phe-Phe and adding a proton on the imidazole nitrogen of the histidine residue.⁷¹ The vibrational spectra were simulated by convoluting the harmonic frequencies obtained at the same level of calculation by a Lorentzian line shape (FWHM 10 cm⁻¹). The harmonic frequencies were scaled by 0.97 in the 800-2000 cm⁻¹ region and 0.955 in the 3000-3800 cm⁻¹ range to account for anharmonicity and basis set incompleteness.⁶⁶ These range-specific scaling factors are identical to those used for other protonated cyclic dipeptides.^{41, 46} They were determined for an analogous DKP peptide, cyclo tyrosine-proline, by the slope of the linear regression of the ratio

between harmonic and anharmonic frequencies obtained for all the computed structures.⁴² Indeed, mode-dependent scaling factors based on an extensive library of systems improve agreement with the experiment.⁷²⁻⁷³ The assignment of the spectra to calculated structures is made based on a good agreement between simulated and experimental spectra and on energetic considerations. An estimation of the conformers populations was given using Boltzmann populations in vacuum at room temperature. However, these numbers must be taken with caution, as discussed below, because of solvation and kinetic trapping effects. All calculations were performed with the Gaussian 09 package.⁷⁴

2.b. Molecular dynamics methods

A detailed picture of the unimolecular dissociation in both diastereomers was obtained through Chemical Molecular Dynamics (MD) simulations. This method is generally called chemical dynamics since the forces are calculated “on the fly” using quantum chemistry, allowing the system to react. This approach, pioneered by Hase and co-workers,⁵⁶ is based on the internal energy activation (E_v) through a microcanonical (NVE) normal mode sampling.⁷⁵ An exhaustive description of the method can be found in the recently published review.⁵⁵ The general chemical dynamics software VENUS⁷⁶ was interfaced with the MOPAC package for electronic structure calculations.⁷⁷ The electronic structure of the systems was solved “on the fly” using the RM1-D semi-empirical Hamiltonian.⁷⁸ This level of theory has shown a good balance between accuracy and computational-time for the computation of theoretical mass spectra.⁷⁹ The most stable isomer found in the static calculations, to which the experimental spectrum was assigned, was chosen as a starting structure for each diastereomer. Seven excess vibrational energies were used for activating c-LDH⁺, namely, 467, 492, 517, 542, 567, 592, and 617 kcal/mol. These high-energy values allow the completion of the time-consuming theoretical breakdown curve in the picosecond time-scale. Therefore, fragmentation is completed in the 25 ps long MD trajectory (see below). Subsequently, to compare the fragmentation of the two diastereomers, a single energy of 517 kcal/mol was used for c-LLH⁺. An ensemble of 11000 trajectories per excess energy was propagated by numerically solving Newton's equation of motion using the velocity Verlet algorithm with a time step (Δt) of 1 fs for a total integration time of 25 ps. This time step ensures proper total energy convergence, *i.e.*, less than 0.20 kcal/mol. The initial rotational energy was sampled according to the Boltzmann distribution at 300K. The analysis of all the trajectories was performed to detect the formation of both intermediate isomers and reaction products. A trajectory was said to be reactive if more than one molecule was identified continuously during 5 ps. The subsequent computation of the time-dependent mass spectrum was obtained following a graph-based theory approach that has been recently developed.^{60 80-81} For different snapshots of the trajectories, we built a distance matrix. Imposing a distance criterion with the parameters used by Jeanvoine *et al.*⁸¹ we obtain the adjacency matrix, the elements of which are 1 if two atoms are linked and 0 otherwise. Using graph-theory algorithms, we can know whether we have a single molecule (so no fragmentation) or more than one (resulting in fragmentation). Furthermore, it is also possible to know whether we have the same structure as the initial one or if bond rearrangement occurs. The present approach cannot distinguish rotamers, but only if bonds are broken and/or made. In this way, it is possible to analyze a huge number of trajectories of complex systems and obtain the key information to identify fragmentation products and associated mechanisms.

2.c. Nomenclature

Figure 1 displays the molecules under study and the dihedral angles τ defining the orientation of the aromatic side chains. Briefly, each benzyl substituent is called in **g**⁺, **g**⁻, or **t** orientation when the value of τ is around 60°, -60°, and 180°. In terms of geometry, the **g**⁺ orientation corresponds to an aromatic ring folded over the dipeptide ring, while **g**⁻ or **t** orientations correspond to extended conformations of the aromatic side chain.

Results and discussion

1. Static Calculations

The most stable structures of c-LLH⁺ and c-LDH⁺ are shown in Figure 2. Their relevant structural parameters are listed in Table 1. They all show protonation on the histidine nitrogen, as expected from its basicity (pK_A=6.0). Although structures with the proton on the oxygen are the most stable in other DKP dipeptides,^{46, 49} they are found much higher in energy here (> 15 kcal/mol). The energy of the structures protonated on the amide NH is even larger (>23 kcal/mol). We will therefore discard these forms and limit the discussion to those protonated on the histidine nitrogen. All the stable structures formed involve a strong NH⁺...O interaction, accompanied by conformer-dependent ancillary interactions as described in what follows.

NH⁺...O/CH...π structures: The most stable structure for both diastereomers is a **g⁺t** geometry, with the benzyl of the phenylalanine folded over the DKP ring and the imidazole of the histidine extended outwards. The **t** orientation of the imidazole substituent optimizes the interaction between the NH⁺ and the amide carbonyl. This results in the formation of a so-called C7 (OC₄C₃C₁₂C₁₃NH) intramolecular hydrogen bond, involving a seven-member ring, which has similar strength for the two diastereomers (d(C₄O...H⁺N)=1.61 Å for c-LL and c-LD alike). **t** orientation of the charged residue was also observed in the cyclo Tyr-Tyr radical cation, as it favors a stabilizing interaction between the amide CO and the charged aromatic ring.⁴⁵ In c-LLH⁺, the two side chains are both in pseudo axial position, allowing the formation of a C_βH...π interaction. In c-LDH⁺, the benzyl is in pseudo axial, and the imidazole is in pseudo equatorial, allowing a C_αH...π interaction. The distance between the hydrogen and the center of the aromatic ring is shorter (2.42 Å) in c-LLH⁺ than in c-LDH⁺ (2.56 Å), suggesting a stronger stabilization of the former, in line with a Gibbs energy difference of 0.76 kcal/mol in favor of c-LLH⁺. This different interaction, C_βH...π vs. C_αH...π, is the major difference between the two diastereomers and was observed previously in neutral or protonated cyclo Phe-Phe.^{44, 46} For both diastereomers, the outwards position of the imidazole is important as it allows forming the CH...π, as already observed for neutral DKP dipeptides with aromatic residues.⁴⁴⁻⁴⁵

NH⁺...O/NH...π structures: The second most stable structure is a **g⁺t** geometry, which shows the same orientation of the imidazole, hence the same NH⁺...O interaction as in the NH⁺...O/CH...π structures described above. In contrast to the NH⁺...O/CH...π structures, the NH⁺...O distance is slightly shorter in c-LLH⁺ (1.59 Å) than in c-LDH⁺ (1.62 Å), in line with higher relative energy in the latter. The **g⁺** orientation of the benzyl facilitates an additional NH...π interaction from the amide NH to the benzyl π cloud. The NH donor belongs to the same amide bond as the CO acting as an acceptor in the NH⁺...O interaction and is more acidic because of this interaction. The NH...π interaction is similar in the two diastereomers with a distance between the hydrogen and the center of the ring of 3.18 and 3.20 Å for c-LDH⁺ and c-LLH⁺, respectively. The different NH⁺...O interaction is the main difference between the two diastereomers. The relative Gibbs energy of the NH...π structure is much larger for c-LLH⁺ (2.23 kcal/mol) than for c-LDH⁺ (1.35 kcal/mol). Consequently, **g⁺t** contributes to 91% vs. 97% in c-LDH⁺ and c-LLH⁺, respectively, while **g⁺t** contributes to 9% in c-LDH⁺ and is negligible in c-LLH⁺.

2. Vibrational Spectra and Assignment

The experimental spectra of c-LLH⁺ and c-LDH⁺ are shown in Figure 3. Their general features are similar in both the fingerprint and the XH stretch regions. However, some differences will be highlighted below. The absence of a band in the 3550-3600 cm⁻¹ range, where the free ν(OH) stretch is expected,^{41, 46, 50} confirms that the observed species is protonated on the histidine nitrogen, as is confirmed by the

presence of strong bands assigned to the imidazole NH bending modes (*vide infra*). Figure 3 also shows the spectra calculated for the most stable structures contributing to more than 5% of the population, *i.e.*, **g⁺t** for c-LLH⁺, or **g⁺t** and **g⁺t** for c-LDH⁺. The interpretation of the experimental spectra in terms of the contribution of these isomers is very satisfactory, as described below. The most intense observed and calculated frequencies are listed in Tables S1 and S2 of the Supplementary Information.

In the fingerprint region, the frequencies are calculated at similar values for the different conformers of the two diastereomers. The experimental spectrum is dominated by three intense bands at ~ 1600, 1660, 1740 cm⁻¹, which appear at identical positions for c-LLH⁺ and c-LDH⁺. The ~1600 cm⁻¹ band is assigned to a mode localized on the imidazole moiety, described in terms of coupled motions of the C=C stretching and NH bending modes. The bands at ~1660 and 1740 are assigned to the bound and free $\nu(\text{CO})$ stretches. The large splitting between them reflects the strong NH⁺...O interaction. The corresponding normal modes involve coupling between CO stretch and NH bend within the same amide bond. Moreover, the bound $\nu(\text{CO})$ is strongly mixed with the histidine bound $\beta(\text{NH})$. The amide II region shows a broad feature with two maxima at ~1435 and ~1395 cm⁻¹ and a sharp intense band at ~1320 cm⁻¹. A clear-cut description of the modes in terms of nuclear motions is difficult in this range because the calculated modes involve coupled motions. The two maxima observed are assigned to modes involving coupled bending motions of the bound histidine NH and the two amide NH. The sharp band is assigned to the coupled motion of the two histidine NH bends. Bands due to the $\beta(\text{CH})$ and $\beta(\text{OH})$ bending modes appear further down in energy. The correspondence between simulated and experimental spectra is less satisfactory, due to the expected anharmonic nature of the modes in this region. However, the bandwidth of the overlapping bands appearing in this range of the experimental spectra (see Figure 3) precludes observing clear cut differences between c-LLH⁺ and c-LDH⁺.

The OPO region is more telling, both in terms of sensitivity to conformation and stereochemical factors. First, different spectra are calculated for the NH⁺...O/CH... π and NH⁺...O/NH... π structures. The strong band observed at 3477 cm⁻¹ is typical of the imidazole free NH stretch with identical frequency in all the calculated conformers of both c-LLH⁺ and c-LDH⁺.⁸² The $\nu(\text{NH})$ stretch free amide, *i.e.* not involved in the NH⁺...O interaction, and the bound amide appears lower in energy: the band at ~3405 cm⁻¹ is assigned to the free amide $\nu(\text{NH})$ stretching modes, calculated at an identical frequency, within 5 cm⁻¹, for all the conformers of both c-LLH⁺ and c-LDH⁺. The sideband that appears at 3370 cm⁻¹ in c-LDH⁺ only is assigned to the bound amide $\nu(\text{NH})$ stretch of the NH⁺...O/NH... π structure, shifted down in energy by the interaction with the benzyl. This band appears only weakly in the experiment, reflecting a minor population of the NH⁺...O/NH... π conformer. According to its Gibbs energy, the room temperature Boltzmann population would be ~10%. Still, the trapped population cannot be determined precisely due to the possibility of kinetic trapping and the modification of energetics between the gas phase and solution.⁸³⁻⁸⁴ Lastly, a band appears at ~3165 cm⁻¹, with unusually large intensity for a $\nu(\text{CH})$ stretch. It is assigned to the asymmetric combination of the two imidazole $\nu(\text{CH})$ stretches. Figure S1 shows the simulated spectrum for the conformers that are not populated in our experimental conditions.

The IRMPD results allow us to conclude that two conformers of c-LDH⁺ coexist in our experimental conditions. This contrasts with c-LLH⁺, for which one conformer is dominant. A larger number of low-energy conformers for the heterochiral diastereomer has been observed already in linear or cyclic peptides^{44, 46} as well as hydrogen-bonded complexes.⁸⁵

3. Collision-Induced Dissociation Fragments and Chemical Dynamic Simulation

The MS² Collision-Induced Dissociation (CID) spectra of c-LLH⁺ and c-LDH⁺, obtained in the hexapole collision cell with a collision voltage of 11 eV, is shown in Figure 4. Identical fragments are observed

for both diastereomers, with however different relative intensities. These differences are much higher than what was observed in previously reported CID experiments on DKP peptides.^{41, 46} Figure 4 also displays the branching ratio corresponding to the different fragments observed, recorded from 1 to 17 V. c-LDH⁺ shows a higher fragmentation yield at all collision energies except the highest one. The chemical dynamics simulations provide tentative structures for all the fragmentation products observed in the MS² spectra. Table 2 lists the *m/z* of the ionic fragments observed experimentally and the molecular formula of the corresponding reaction products (for both ions and neutrals) obtained from simulations. Figure 5 shows the most abundant isomer for each *m/z* product obtained from chemical dynamics simulations. The structure of the corresponding neutral fragments is given in Figure S2 of the supporting information. These structures have to be taken cautiously due to the time scale differences between simulations (ps) and experiment (ms).

The analysis of the ensemble of trajectories obtained from the chemical dynamics simulations is performed to assign the *m/z* peaks observed in the MS² spectrum resulting from collision-induced dissociation. Comparison between the results obtained for c-LLH⁺ and c-LDH⁺ aims to shed light on the role of the histidine residue on stereochemical effects.

The dominant fragmentation channels are loss of ammonia NH₃ (*m/z* 268 C₁₅H₁₄N₃O₂⁺), carbon monoxide CO (*m/z* 257 C₁₄H₁₇N₄O⁺) and formation of *m/z* 212 (C₁₃H₁₄N₃⁺), which corresponds to the loss of CO and HCONH₂ or 2CO and NH₃. The branching ratios as a function of energy (Figure 4) show that this sequential fragmentation occurs even at low collision voltage. Interestingly, the fragment corresponding to the phenylalanine iminium ion (*m/z* 120 C₈H₁₀N⁺), which dominates the CID spectrum of cyclo Phe-PheH⁺,⁴⁶ is very weak, at the detection limit, in cyclo His-PheH⁺, as is the histidine iminium ion (*m/z* 110 C₅H₈N₃⁺). Instead, the dominant channel is the formation of *m/z* 212, as previously mentioned. This channel is also an important fragmentation pathway in most DKP dipeptides studied so far, including protonated aromatic DKP peptides like cyclo Phe-Phe (*m/z* 222)⁴⁶ or cyclo Tyr-Pro (*m/z* 188).^{41, 86-88} At larger collision energy, sequential fragmentation is observed, like subsequent loss of CO or NH₃ from *m/z* 268 or *m/z* 257, respectively, to form *m/z* 240 (C₁₄H₁₄N₃O⁺). Other minor peaks are identified, such as the dehydration channel at *m/z* 267 (C₁₅H₁₅N₄O⁺) and the subsequent loss of the isocyanic acid from it, *m/z* 224 (C₁₄H₁₄N₃⁺). The peak at *m/z* 166 (C₇H₈O₂N₃⁺) is assigned mainly to the loss of a toluene isomer plus hydrogen cyanide molecule from the parent ion. Direct fragmentation events due to the cleavage of C_α-C_β bonds are also identified but they are energetically disfavored. Protonation of the amide nitrogen weakens the corresponding amide bond.⁸⁹ As a result, the C-N bond is expected to break first, while the C_α-C_β being further from the protonation site and much less affected by the nitrogen protonation will demand more energy to break. *m/z* 193 (C₈H₉N₄O₂⁺), 194 (C₈H₁₀N₄O₂⁺), and 195 (C₈H₁₁N₄O₂⁺) result from the C_α-C_β cleavage of the Phe residue (C₁-C₅ in Figure 1) while *m/z* 203 and 204 result from the C_α-C_β cleavage of the His residue (C₃-C₁₂ in Figure 1). According to the experimental findings, the C_α-C_β cleavage is favored in the Phe residue compared to the His residue.

4. Diastereomeric Discrimination in Collision-Induced Dissociation

The total fragmentation efficiency is larger for cyclo LDH⁺ than cyclo LLH⁺. This is reminiscent of what was observed in protonated cyclo diphenylalanine.⁴⁶ However, the effect is much more pronounced here. The threshold for secondary fragmentation (loss of CO and NH₃) is higher by 2V in c-LLH⁺ than c-LDH⁺, pointing towards a lower fragmentation threshold for c-LDH⁺. At low energy, the branching ratio is higher for all fragments but NH₃ loss, which suggests that in c-LDH⁺, the primary fragment formed by NH₃ loss is less stable and more prone to undergo secondary fragmentation. Loss of CO is particularly

dependent upon chirality and is more efficient in c-LDH⁺ at all collision energies studied. A factor of ~3 between the two diastereomers appears at 11 V.

We suggest that the stronger effect of chirality observed here is due to the proton mobility in a diastereomer-sensitive region before the dissociation occurs. We also suggest that the difference observed is strongly related to the proton position in the reagent, which is the amide CO in cyclo Phe-PheH⁺ and cyclo Tyr-ProH⁺, and the histidine nitrogen in cyclo His-PheH⁺. To test this hypothesis, we perform a dedicated analysis of the trajectories. The comparison between c-LLH⁺ and c-LDH⁺ is facilitated because the energy difference between the two structures is small. Therefore, the simulations allow assessing the effect of the sole relative absolute configuration of the residues on the proton mobility without being influenced by different excess energies.

Figure 6 (left panel) compares the probability of obtaining reactive trajectories as a function of the integration time at 517 kcal/mol of vibrational excess energy for the two diastereomers. c-LDH⁺ shows a larger fragmentation yield than its counterpart c-LLH⁺, as experimentally observed. Figure 6 (right panel) shows the formation yield of *m/z* 257, *i.e.*, CO loss, as a function of time, indicating that c-LDH⁺ displays a slightly higher yield than its counterpart c-LLH⁺, a point on which we shall focus later in the discussion. As mentioned before, experimental and theoretical absolute values cannot be directly compared because of the differences in time scales. Nevertheless, the analysis of the ensemble of trajectories under fragmentation conditions that lead to the experimentally obtained fragments allows us to propose some hypotheses on the role of the histidine in the stereochemical effects observed in the CID. The MD simulations evidence the presence of intermediate states called “intermediate isomers” in what follows. They will be denoted ISO_{*i*} with *i*=1-9, in the order of decreasing frequency of appearance in the chemical dynamics trajectory. To our surprise, one of them (ISO6) was calculated as more stable than the reagent. Therefore, we have checked that it was not the species observed in the IRMPD experiments by comparing its simulated spectrum to the experiment (see Figure S1). The main intermediate isomers populated prior to dissociation are shown in Figure 7 for c-LDH⁺ and c-LDH⁺. Their optimized geometry are given in Figure S3 of the SI. They correspond to the intermediate states that appear the most frequently in the MD trajectories, whatever the issue of the trajectory and the reaction product. They can be divided into two main groups. Group 1, shown at the top of Figure 7, encompasses those intermediate isomers that contain two asymmetric carbons. These isomers are non predissociated, *i.e.* with an intact peptide ring. It should be noted that ISO1, ISO4, ISO5, and ISO9 are tautomers and only differ by the position of the proton. All these intermediate states exist in two diastereomeric forms LL or LD. Physically, their existence results from the histidine proton migration to the peptide ring before it opens up. Most of the time, when the activated reactive structure is c-LLH⁺, the main intermediate isomers reached in the Group 1 region are LL isomers. Similarly, activation of c-LDH⁺ mostly results in the LD intermediate isomers. Nevertheless, the opposite happens in a few trajectories through exchange of the alpha-hydrogen atom. In contrast, Group 2, shown at the bottom of Figure 7, contains intermediate isomers with a single asymmetric carbon L or D. All these isomers except ISO2 are predissociated intermediate states, *i.e.* the DKP ring opens up. In this group, ISO3, ISO7 and ISO8 only differ by the location of the proton. Each intermediate isomer in Group 2 exists in two isoenergetic enantiomers. In Group 1, the LL and LD diastereomers are endowed with different relative energy and barriers to dissociation. Our working hypothesis is that the sensitivity of the reaction to stereochemical factors will strongly depend on which of these regions (Group 1 or 2) of the PES is visited during the reaction. Once the systems arrive in the Group 2 region, all the barriers to fragmentation are identical whether the parent is c-LLH⁺ or c-LDH⁺. It means that the stereochemical effect on the reaction is related only to what happens before reaching this zone. Therefore, the

diastereomeric discrimination strongly depends on the time the system spends in the Group 1 region, as schematically described in Figure 8. Two reaction paths with different sensitivity to stereochemical factors can thus be expected in the CID experiments. The first one, shown by a black arrow in Figure 8, represents those trajectories that isomerize directly to the Group 2 region before dissociation. This is the case for the NH_3 loss reaction shown in Figure 9. The first reaction step deduced from chemical dynamics simulations is a hydrogen transfer from the histidine C_α to the histidine amide NH, which in turn results in the opening of the DKP peptide ring. In this case, stereochemical factors will only affect the first step where the system goes from the reactant to the Group 2 region (mechanism A). Therefore, the expected stereochemical effects will be small, as observed for the CID of protonated cyclo Tyr-Pro.⁴¹ In the other case, shown by a red arrow in Figure 8, the system evolves in the Group 1 region (mechanism B), sensitive to stereochemical factors. This is the case for the CO loss reaction shown in Figure 9. The first reaction step evidenced in chemical dynamics simulations is the migration of a proton from the imidazole nitrogen to one of the amide nitrogens. The ring opening necessary for CO loss only happens after this stereochemistry-sensitive step. The chirality effect is thus expected to be much more pronounced.

The mechanism A is predominant in systems like protonated cyclo Tyr-Pro and protonated cyclo Phe-Phe and this is why a very moderate dependence upon diastereoisomer is observed in CID. In these cases, the main isomerization pathways happen in the Group 2 region. This is related to the fact that the proton is primarily localized on the amide CO and that the first reaction step is proton migration on the amide NH followed by the cleavage of the N-C^+ bond.⁴¹

The mechanism B is predominant in protonated cyclo His-Phe and is linked to the presence of the histidine residue, whose imidazole ring is the protonation site. To illustrate this, we will qualitatively describe the two main pathways for CO loss based on the chemical dynamics trajectories. In both reaction paths (see figure 9), the loss occurs after a proton migration from the imidazole to one of the two amide nitrogen atoms in the DKP ring, weakening the N-C_2 or N-C_4 bond. This leads to ISO4 and ISO9 of Figure 7, respectively, and results in the ejection of the corresponding CO group. The imidazole ring transfers the proton to the new protonation site. The analysis of the trajectories indicates that the proton always leaves from the imidazole NH^+ that is the closest to the peptide ring. The presence of tautomers, as mentioned above, facilitates the proton mobility by giving the system the “choice” of the favorable, *i.e.*, closest, proton position, which are indicated by the red and green arrows in Figure 9. Still, this proton transfer demands some molecular reorganization, more precisely rotation of the imidazole substituent. This rotation-induced proton mobility is very sensitive to the stereochemistry of the reagent. In c-LLH^+ the two aromatic rings are on the same side of the DKP ring. Therefore, the steric clash between the aromatic rings makes the rotation difficult, which in turn decreases the proton mobility efficiency. In contrast, in c-LDH^+ the two aromatic rings are on opposite sides of the peptide ring, which might facilitate easier proton transfer to the amide nitrogen in the DKP ring compared to c-LLH^+ . The effects seen here arise then from two contributions: first, protonation happens on the imidazole, so that a mechanism consisting of a proton migration to the ring is necessary. This mechanism is reminiscent of that observed in histidine-containing peptides³³. Second, the phenyl ring introduces diastereoselective steric hindrance, hence a barrier to proton mobility. The conjunction of these two factors forces the system to visit the Group 1 region, sensitive to chirality. As a result, high diastereomeric discrimination is observed. In conclusion NH_3 loss (mechanism A) and CO loss (mechanism B) show very different sensitivity upon stereochemical factors in protonated cyclo His-Phe, as shown in Figure 9, because the first step involves opening of the peptide ring (mechanism A) or preserves the cyclic structure (mechanism B), respectively.

Conclusion

IRMPD spectroscopy evidenced that the two diastereomers of protonated cyclo His-Phe display identical most stable $\mathbf{g}^{\dagger}\mathbf{t}$ structure, protonated on the histidine nitrogen, with the benzyl of the phenylalanine folded over the DKP ring. The imidazole of the histidine has an extended conformation, which allows the formation of a stabilizing $\text{NH}^{\dagger}\dots\text{O}$ interaction. A weaker $\text{CH}\dots\pi$ interaction also contributes to the stability, which is reminiscent of the structure of neutral DKP dipeptides with aromatic residues.⁴⁴⁻⁴⁵ A higher-energy $\mathbf{g}^{\dagger}\mathbf{t}$ structure is populated (<10%) for c-LDH⁺ only, with the benzyl ring extended over the DKP ring. This geometry allows an $\text{NH}\dots\pi$ interaction to take place, which manifest itself by the presence of an additional weak absorption band in the region of the NH stretch, compared to c-LLH⁺. The increased flexibility of the heterochiral system has been observed previously in other biomolecules or complexes.^{27, 46, 85} The two diastereomers differ in their collision-induced fragmentation efficiency much more than previously observed for other protonated DKP peptides like cyclo Tyr-Pro or cyclo Phe-Phe.^{41, 46} Chemical dynamics simulations explain this observation in terms of competition between two different mechanisms, which are sketched in Figure 9. One of them is dominant for NH_3 loss and involves mostly predissociated intermediate states (Group 2), *i.e.* intermediate states in which the opening of the DKP ring results in the presence of only one asymmetric carbon. This happens through the migration of a hydrogen atom from the C_α of the histidine to the amide nitrogen of the same residue, with concomitant ring opening. Then, the proton initially located on the basic imidazole nitrogen migrates to the amide nitrogen of the histidine residue, followed by NH_3 loss. Therefore, the barrier to the formation of this intermediate is therefore identical for the two diastereomers, which makes the reaction insensitive to chirality. The other mechanism involves non-predissociated intermediate states (Group 1), *i.e.* intermediate states that keep the DKP ring intact, with two asymmetric carbon atoms. These stereogenic centers can be of identical or opposite absolute configurations, depending on the configuration of the reactant, and thus differ in energy for the two diastereomers. This stereoselective mechanism dominates for CO loss. It requires a proton migration from the initially protonated imidazole to the peptide ring. The proton mobility is facilitated by the fact that the two tautomers of imidazole are evidenced as intermediate isomers. As a result, the transfer of the proton to the peptide ring happens in the tautomer in which the distance between the proton and the ring is the smallest one. Mobility of the proton happens before the ring opens up, which is the reason why chirality effects are observed: the reaction has to go through a barrier due to the rotation of the imidazole substituent, which is different in c-LLH⁺ and c-LDH⁺. These results contrast with what was observed in cyclo-Gly-GlyH⁺, in which the peptide ring opens first and then isomerizes. In systems like cyclo Tyr-ProH⁺ and cyclo Phe-PheH⁺, such a mechanism is also dominant, explaining the limited chirality effects observed. The study of protonated cyclo His-His could help confirm this hypothesis and is planned in the near future.

Acknowledgements

We thank Dr. J. M. Ortega and the CLIO team for technical assistance and Dr. D. Scuderi for helpful discussions. We thank F. Gobert for experimental help. We acknowledge the use of the computing facility cluster MésoLUM of the LUMAT federation (FR LUMAT 2764). AFPM and RS thank ANR DynBioReact (Grant No. ANR-14-CE06-0029-01) for financial support. The research described here has been supported by the Investissements d'Avenir LabEx PALM contract (ANR-10-LABX-0039-PALM).

References

1. Ward, T. J.; Ward, K. D. Chiral Separations: A Review of Current Topics and Trends. *Analytical Chemistry* **2012**, *84* (2), 626-635.
2. Shukla, A. K.; Futrell, J. H. Tandem mass spectrometry: dissociation of ions by collisional activation. *Journal of Mass Spectrometry* **2000**, *35* (9), 1069-1090.
3. Wells, J. M.; McLuckey, S. A. Collision-induced dissociation (CID) of peptides and proteins. In *Biological Mass Spectrometry*, Burlingame, A. L., Ed. 2005; Vol. 402, pp 148-185.
4. Tsaprailis, G.; Nair, H.; Somogyi, A.; Wysocki, V. H.; Zhong, W. Q.; Futrell, J. H.; Summerfield, S. G.; Gaskell, S. J. Influence of secondary structure on the fragmentation of protonated peptides. *Journal of the American Chemical Society* **1999**, *121* (22), 5142-5154.
5. Zubarev, R. A. Reactions of polypeptide ions with electrons in the gas phase. *Mass Spectrometry Reviews* **2003**, *22* (1), 57-77.
6. Paizs, B.; Suhai, S. Fragmentation pathways of protonated peptides. *Mass Spectrometry Reviews* **2005**, *24* (4), 508-548.
7. Sudha, R.; Jarrold, M. F. Left-handed and ambidextrous helices in the gas phase. *Journal of Physical Chemistry B* **2005**, *109* (23), 11777-11780.
8. Domalain, V.; Tognetti, V.; Hubert-Roux, M.; Lange, C. M.; Joubert, L.; Baudoux, J.; Rouden, J.; Afonso, C. Role of Cationization and Multimers Formation for Diastereomers Differentiation by Ion Mobility-Mass Spectrometry. *J. Am. Soc. Mass Spectrom.* **2013**, *24* (9), 1437-1445.
9. Wysocki, V. H.; Tsaprailis, G.; Smith, L. L.; Brechi, L. A. Special feature: Commentary - Mobile and localized protons: a framework for understanding peptide dissociation. *Journal of Mass Spectrometry* **2000**, *35* (12), 1399-1406.
10. Frison, G.; van der Rest, G.; Turecek, F.; Besson, T.; Lemaire, J.; Maitre, P.; Chamot-Rooke, J. Structure of Electron-Capture Dissociation Fragments from Charge-Tagged Peptides Probed by Tunable Infrared Multiple Photon Dissociation. *Journal of the American Chemical Society* **2008**, *130* (45), 14916-+.
11. Adams, C. M.; Kjeldsen, F.; Zubarev, R. A.; Budnik, B. A.; Haselmann, K. F. Electron capture dissociation distinguishes a single D-amino acid in a protein and probes the tertiary structure. *J. Am. Soc. Mass Spectrom.* **2004**, *15* (7), 1087-1098.
12. Zehnacker, A. Chirality Effects in Gas-Phase Spectroscopy and Photophysics of Molecular and Ionic Complexes: Contribution of Low and Room Temperature Studies. *International Reviews in Physical Chemistry* **2014**, *33* (2), 151-207.
13. Kumar, S.; Lucas, B.; Fayeton, J.; Scuderi, D.; Alata, I.; Broquier, M.; Le Barbu-Debus, K.; Lepere, V.; Zehnacker, A. Photofragmentation mechanisms in protonated chiral cinchona alkaloids. *Physical Chemistry Chemical Physics* **2016**, *18* (32), 22668-22677.
14. Scuderi, D.; Maitre, P.; Rondino, F.; Le Barbu-Debus, K.; Lepere, V.; Zehnacker-Rentien, A. Chiral Recognition in Cinchona Alkaloid Protonated Dimers: Mass Spectrometry and UV Photodissociation Studies. *Journal of Physical Chemistry A* **2010**, *114* (9), 3306-3312.
15. Rijs, A. M.; Oomens, J. *Gas-Phase IR Spectroscopy and Structure of Biological Molecules*. Springer International Publishing: 2015.
16. Sediki, A.; Snoek, L. C.; Gageot, M. P. N-H⁺ vibrational anharmonicities directly revealed from DFT-based molecular dynamics simulations on the Ala(γ)H(⁺) protonated peptide. *International Journal of Mass Spectrometry* **2011**, *308* (2-3), 281-288.
17. Polfer, N. C. Infrared Multiple Photon Dissociation Spectroscopy of Trapped Ions. *Chemical Society Reviews* **2011**, *40* (5), 2211-2221.

18. Polfer, N. C.; Oomens, J.; Suhai, S.; Paizs, B. Infrared spectroscopy and theoretical studies on gas-phase protonated leu-enkephalin and its fragments: Direct experimental evidence for the mobile proton. *Journal of the American Chemical Society* **2007**, *129* (18), 5887-5897.
19. Scutelnic, V.; Perez, M. A. S.; Marianski, M.; Warnke, S.; Gregor, A.; Rothlisberger, U.; Bowers, M. T.; Baldauf, C.; von Helden, G.; Rizzo, T. R.; Seo, J. The Structure of the Protonated Serine Octamer. *Journal of the American Chemical Society* **2018**, *140* (24), 7554-7560.
20. Bythell, B. J.; Maitre, P.; Paizs, B. Cyclization and Rearrangement Reactions of a(n) Fragment Ions of Protonated Peptides. *Journal of the American Chemical Society* **2010**, *132* (42), 14766-14779.
21. Poutsma, J. C.; Martens, J.; Oomens, J.; Maitre, P.; Steinmetz, V.; Bernier, M.; Jia, M. X.; Wysocki, V. Infrared Multiple-Photon Dissociation Action Spectroscopy of the b(2)(+) Ion from PPG: Evidence of Third Residue Affecting b(2)(+) Fragment Structure. *J. Am. Soc. Mass Spectrom.* **2017**, *28* (7), 1482-1488.
22. Correia, C. F.; Balaj, P. O.; Scuderi, D.; Maitre, P.; Ohanessian, G. Vibrational signatures of protonated, phosphorylated amino acids in the gas phase. *Journal of the American Chemical Society* **2008**, *130* (11), 3359-3370.
23. Maitre, P.; Scuderi, D.; Corinti, D.; Chiavarino, B.; Crestoni, M. E.; Fornarini, S. Applications of Infrared Multiple Photon Dissociation (IRMPD) to the Detection of Posttranslational Modifications. *Chemical Reviews* **2020**, *120* (7), 3261-3295.
24. Crestoni, M. E.; Chiavarino, B.; Scuderi, D.; Di Marzio, A.; Fornarini, S. Discrimination of 4-Hydroxyproline Diastereomers by Vibrational Spectroscopy of the Gaseous Protonated Species. *Journal of Physical Chemistry B* **2012**, *116* (30), 8771-8779.
25. Dunbar, R. C.; Steill, J. D.; Oomens, J. Conformations and vibrational spectroscopy of metal-ion/polyalanine complexes. *International Journal of Mass Spectrometry* **2010**, *297* (1-3), 107-115.
26. Dunbar, R. C.; Steill, J. D.; Oomens, J. Chirality-Induced Conformational Preferences in Peptide-Metal Ion Binding Revealed by IR Spectroscopy. *Journal of the American Chemical Society* **2011**, *133* (5), 1212-1215.
27. Lepere, V.; Le Barbu-Debus, K.; Clavaguéra, C.; Scuderi, D.; Piani, G.; Simon, A.-L.; Chirot, F.; MacAleese, L.; Dugourd, P.; Zehnacker, A. Chirality-dependent structuration of protonated or sodiated polyphenylalanines: IRMPD and ion mobility studies. *Physical Chemistry Chemical Physics* **2016**, *18* (3), 1807-17.
28. Brodbelt, J. S. Ion Activation Methods for Peptides and Proteins. *Analytical Chemistry* **2016**, *88* (1), 30-51.
29. Bleiholder, C.; Osburn, S.; Williams, T. D.; Suhai, S.; Van Stipdonk, M.; Harrison, A. G.; Paizs, B. Sequence-Scrambling Fragmentation Pathways of Protonated Peptides. *Journal of the American Chemical Society* **2008**, *130* (52), 17774-17789.
30. Bythell, B. J.; Suhai, S.; Somogyi, A.; Paizs, B. Proton-Driven Amide Bond-Cleavage Pathways of Gas-Phase Peptide Ions Lacking Mobile Protons. *Journal of the American Chemical Society* **2009**, *131* (39), 14057-14065.
31. Harrison, A. G.; Young, A. B.; Bleiholder, C.; Suhai, S.; Paizs, B. Scrambling of sequence information in collision-induced dissociation of peptides. *Journal of the American Chemical Society* **2006**, *128* (32), 10364-10365.
32. Chu, I. K.; Siu, C. K.; Lau, J. K. C.; Tang, W. K.; Mu, X. Y.; Lai, C. K.; Guo, X. H.; Wang, X.; Li, N.; Xia, Y.; Kong, X. L.; Oh, H. B.; Ryzhov, V.; Turecek, F.; Hopkinson, A. C.; Siu, K. W. M. Proposed nomenclature for peptide ion fragmentation. *International Journal of Mass Spectrometry* **2015**, *390*, 24-27.
33. Tsaprailis, G.; Nair, H.; Zhong, W.; Kuppannan, K.; Futrell, J. H.; Wysocki, V. H. A mechanistic investigation of the enhanced cleavage at histidine in the gas-phase dissociation of protonated peptides. *Analytical Chemistry* **2004**, *76* (7), 2083-2094.
34. Gucinski, A. C.; Chamot-Rooke, J.; Nicol, E.; Somogyi, A.; Wysocki, V. H. Structural Influences on Preferential Oxazolone versus Diketopiperazine b(2)(+) Ion Formation for Histidine Analogue-Containing Peptides. *Journal of Physical Chemistry A* **2012**, *116* (17), 4296-4304.

35. Huang, Y. Y.; Wysocki, V. H.; Tabb, D. L.; Yates, J. R. The influence of histidine on cleavage C-terminal to acidic residues in doubly protonated tryptic peptides. *International Journal of Mass Spectrometry* **2002**, *219* (1), 233-244.
36. Alauddin, M.; Gloaguen, E.; Brenner, V.; Tardivel, B.; Mons, M.; Zehnacker-Rentien, A.; Declerck, V.; Aitken, D. J. Intrinsic Folding Proclivities in Cyclic -Peptide Building Blocks: Configuration and Heteroatom Effects Analyzed by Conformer-Selective Spectroscopy and Quantum Chemistry. *Chemistry-a European Journal* **2015**, *21* (46), 16479-16493.
37. Mahjoub, A.; Chakraborty, A.; Lepere, V.; Le Barbu-Debus, K.; Guchhait, N.; Zehnacker, A. Chirality-dependent hydrogen bond direction in jet-cooled (S)-1,2,3,4-tetrahydro-3-isoquinoline methanol (THIQM): IR-ion dip vibrational spectroscopy of the neutral and the ion. *Physical Chemistry Chemical Physics* **2009**, *11* (25), 5160-5169.
38. Bouchet, A.; Klyne, J.; Piani, G.; Dopfer, O.; Zehnacker, A. Diastereo-Specific Conformational Properties of Neutral, Protonated and Radical Cation Forms of (1R,2S)-cis and (1R,2R)-trans Amino-Indanol by Gas Phase Spectroscopy. *Physical Chemistry Chemical Physics* **2015**, *17*, 25809-25821.
39. Prasad, C. BIOACTIVE CYCLIC DIPEPTIDES. *Peptides* **1995**, *16* (1), 151-164.
40. Bellezza, I.; Peirce, M. J.; Minelli, A. Cyclic dipeptides: from bugs to brain. *Trends in Molecular Medicine* **2014**, *20* (10), 551-558.
41. Pérez Mellor, A.; Alata, I.; Lepère, V.; Zehnacker, A. Stereospecific Collision-Induced Dissociation and Vibrational Spectroscopy of Protonated Cyclo (Tyr-Pro). *Accepted for publication in the International Journal for Mass Spectrometry*.
42. Perez-Mellor, A.; Alata, I.; Lepere, V.; Zehnacker, A. Conformational Study of the Jet-Cooled Diketopiperazine Peptide Cyclo Tyrosyl-Prolyl. *Journal of Physical Chemistry B* **2019**, *123* (28), 6023-6033.
43. Pérez Mellor, A.; Zehnacker, A. Chirality Effects in Jet-Cooled Cyclic Dipeptides. In *Physical Chemistry of Cold Gas-Phase Functional Molecules and Clusters*, Ebata, T.; Fujii, M., Eds. Springer: Singapore, 2019; pp 63-87.
44. Perez-Mellor, A.; Alata, I.; Lepere, V.; Zehnacker, A. Chirality effects in the structures of jet-cooled bichromophoric dipeptides. *Journal of Molecular Spectroscopy* **2018**, *349*, 71-84.
45. BenNasr, F.; Perez-Mellor, A.; Alata, I.; Lepere, V.; Jaidane, N. E.; Zehnacker, A. Stereochemistry-dependent hydrogen bonds stabilise stacked conformations in jet-cooled cyclic dipeptides: (LD) vs. (LL) cyclo tyrosine-tyrosine. *Faraday Discussions* **2018**, *212*, 399-419.
46. Alata, I.; Perez-Mellor, A.; Ben Nasr, F.; Scuderi, D.; Steinmetz, V.; Gobert, F.; Jaidane, N. E.; Zehnacker-Rentien, A. Does the Residues Chirality Modify the Conformation of a Cyclo-Dipeptide? Vibrational Spectroscopy of Protonated Cyclo-diphenylalanine in the Gas Phase. *Journal of Physical Chemistry A* **2017**, *121* (38), 7130-7138.
47. Wiedemann, S.; Metsala, A.; Nolting, D.; Weinkauff, R. The dipeptide cyclic(glycyltryptophanyl) in the gas phase: A concerted action of density functional calculations, S-0-S-1 two-photon ionization, spectral UV/UV hole burning and laser photoelectron spectroscopy. *Physical Chemistry Chemical Physics* **2004**, *6* (10), 2641-2649.
48. Abo-Riziq, A. G.; Crews, B.; Bushnell, J. E.; Callahan, M. P.; De Vries, M. S. Conformational analysis of cyclo(Phe-Ser) by UV-UV and IR-UV double resonance spectroscopy and ab initio calculations. *Molecular Physics* **2005**, *103* (11-12), 1491-1495.
49. Wang, D.; Gulyuz, K.; Stedwell, C. N.; Polfer, N. C. Diagnostic NH and OH Vibrations for Oxazolone and Diketopiperazine Structures: b(2) from Protonated Triglycine. *J. Am. Soc. Mass Spectrom.* **2011**, *22* (7), 1197-1203.
50. Zou, S.; Oomens, J.; Polfer, N. C. Competition between diketopiperazine and oxazolone formation in water loss products from protonated ArgGly and GlyArg. *International Journal of Mass Spectrometry* **2012**, *316*, 12-17.
51. Bernier, M. C.; Chamot-Rooke, J.; Wysocki, V. H. R vs. S fluoroproline ring substitution: trans/cis effects on the formation of b(2) ions in gas-phase peptide fragmentation. *Physical Chemistry Chemical Physics* **2016**, *18* (3), 2202-2209.

52. Perkins, B. R.; Chamot-Rooke, J.; Yoon, S. H.; Gucinski, A. C.; Somogyi, A.; Wysocki, V. H. Evidence of Diketopiperazine and Oxazolone Structures for HA b(2)⁽⁺⁾ Ion. *Journal of the American Chemical Society* **2009**, *131* (48), 17528-17529.
53. Cautereels, J.; Giribaldi, J.; Enjalbal, C.; Blockhuys, F. Quantum chemical mass spectrometry: Ab initio study of b(2)-ion formation mechanisms for the singly protonated Gln-His-Ser tripeptide. *Rapid Communications in Mass Spectrometry* **2020**, *34* (12).
54. Shek, P. Y. I.; Lau, J. K.-C.; Zhao, J.; Grzetic, J.; Verkerk, U. H.; Oomens, J.; Hopkinson, A. C.; Siu, K. W. M. Fragmentations of protonated cyclic-glycylglycine and cyclic-alanylalanine. *International Journal of Mass Spectrometry* **2012**, *316*, 199-205.
55. Somer, A. M.; Macaluso, V.; Barnes, G. L.; Yang, L.; Pratihari, S.; Song, K.; Hase, W. L.; Spezia, R. Role of Chemical Dynamics Simulations in Mass Spectrometry Studies of Collision-Induced Dissociation and Collisions of Biological Ions with Organic Surfaces. *J. Am. Soc. Mass Spectrom.* **2020**, *31* (1), 2-24.
56. Meroueh, S. O.; Wang, Y. F.; Hase, W. L. Direct dynamics Simulations of collision- and surface-induced dissociation of N-protonated glycine. Shattering fragmentation. *Journal of Physical Chemistry A* **2002**, *106* (42), 9983-9992.
57. Spezia, R.; Martens, J.; Oomens, J.; Song, K. Collision-induced dissociation pathways of protonated Gly(2)NH(2) and Gly(3)NH(2) in the short time-scale limit by chemical dynamics and ion spectroscopy. *International Journal of Mass Spectrometry* **2015**, *388*, 40-52.
58. Ortiz, D.; Martin-Gago, P.; Riera, A.; Song, K.; Salpin, J. Y.; Spezia, R. Gas-phase collision induced dissociation mechanisms of peptides: Theoretical and experimental study of N-formylalanylamide fragmentation. *International Journal of Mass Spectrometry* **2013**, *335*, 33-44.
59. Macaluso, V.; Scuderi, D.; Crestoni, M. E.; Fornarini, S.; Corinti, D.; Dalloz, E.; Martinez-Nunez, E.; Hase, W. L.; Spezia, R. L-Cysteine Modified by S-Sulfation: Consequence on Fragmentation Processes Elucidated by Tandem Mass Spectrometry and Chemical Dynamics Simulations. *Journal of Physical Chemistry A* **2019**, *123* (17), 3685-3696.
60. Pérez Mellor, A.; Spezia, R. Determination of kinetic properties in unimolecular dissociation of complex systems from graph-theory based analysis of an ensemble of reactive trajectories. *Manuscript in preparation*.
61. Maitre, P.; Le Caer, S.; Simon, A.; Jones, W.; Lemaire, J.; Mestdagh, H.; Heninger, M.; Mauclair, G.; Boissel, P.; Prazeres, R.; Glotin, F.; Ortega, J. M. Ultrasensitive first coupling of FTICR and FEL. *Nucl. Instrum. Methods, Sect. A* **2003**, *507*, 541-546.
62. Prazeres, R.; Glotin, F.; Insa, C.; Jaroszynski, D. A.; Ortega, J. M. Two-colour operation of a Free-Electron Laser and applications in the mid-infrared. *European Physical Journal D* **1998**, *3* (1), 87-93.
63. Bakker, J. M.; Besson, T.; Lemaire, J.; Scuderi, D.; Maitre, P. Gas-phase structure of a pi-allyl-palladium complex: Efficient infrared Spectroscopy in a 7 T Fourier transform mass spectrometer. *Journal of Physical Chemistry A* **2007**, *111* (51), 13415-13424.
64. Marta, R. A.; Wu, R. H.; Eldridge, K. R.; Martens, J. K.; McMahon, T. B. The sodium cation-bound dimer of theophylline: IRMPD spectroscopy of a highly symmetric electrostatically bound species. *International Journal of Mass Spectrometry* **2010**, *297* (1-3), 76-84.
65. Becke, A. D. DENSITY-FUNCTIONAL EXCHANGE-ENERGY APPROXIMATION WITH CORRECT ASYMPTOTIC-BEHAVIOR. *Physical Review A* **1988**, *38* (6), 3098-3100.
66. Halls, M. D.; Velkovski, J.; Schlegel, H. B. Harmonic frequency scaling factors for Hartree-Fock, S-VWN, B-LYP, B3-LYP, B3-PW91 and MP2 with the Sadlej pVTZ electric property basis set. *Theoretical Chemistry Accounts* **2001**, *105*, 413.
67. Frisch, M. J.; Pople, J. A.; Binkley, J. S. Self-Consistent Molecular-Orbital Methods .25. Supplementary Functions for Gaussian-Basis Sets. *Journal of Chemical Physics* **1984**, *80* (7), 3265-3269.
68. Goerigk, L.; Grimme, S. A thorough benchmark of density functional methods for general main group thermochemistry, kinetics, and noncovalent interactions. *Physical Chemistry Chemical Physics* **2011**, *13* (14), 6670-6688.

69. Grimme, S.; Antony, J.; Ehrlich, S.; Krieg, H. A consistent and accurate ab initio parametrization of density functional dispersion correction (DFT-D) for the 94 elements H-Pu. *Journal of Chemical Physics* **2010**, *132* (15), 154104
70. Mohan, N.; Vijayalakshmi, K. P.; Koga, N.; Suresh, C. H. Comparison of Aromatic NH ... π , OH ... π , and CH ... π Interactions of Alanine Using MP2, CCSD, and DFT Methods. *Journal of Computational Chemistry* **2010**, *31* (16), 2874-2882.
71. Perez-Mellor, A.; Zehnacker, A. Vibrational circular dichroism of a 2,5-diketopiperazine (DKP) peptide: Evidence for dimer formation in cyclo LL or LD diphenylalanine in the solid state. *Chirality* **2017**, *29* (2), 89-96.
72. Gloaguen, E.; Mons, M. Isolated Neutral Peptides. In *Gas-Phase Ir Spectroscopy and Structure of Biological Molecules*, Rijs, A. M.; Oomens, J., Eds. 2015; Vol. 364, pp 225-270.
73. Plowright, R. J.; Gloaguen, E.; Mons, M. Compact Folding of Isolated Four-Residue Neutral Peptide Chains: H-Bonding Patterns and Entropy Effects. *ChemPhysChem* **2011**, *12* (10), 1889-1899.
74. Frisch, M. J.; Trucks, G. W.; Schlegel, H. B.; Scuseria, G. E.; Robb, M. A.; Cheeseman, J. R.; Scalmani, G.; Barone, V.; Mennucci, B.; Petersson, G. A.; Nakatsuji, H.; Caricato, M.; Li, X. J.; Hratchian, H. P.; Izmaylov, A. F.; Bloino, J.; Zheng, G.; Sonnenberg, J. L.; Hada, M.; Ehara, M.; Toyota, K.; Fukuda, R.; Hasegawa, J.; Ishida, M.; Nakajima, T.; Honda, Y.; Kitao, O.; Nakai, H.; Vreven, T.; Montgomery, J., J. A.; Peralta, J. E.; Ogliaro, F.; Bearpark, M.; Heyd, J. J.; Brothers, E.; Kudin, K. N.; Staroverov, V. N.; Kobayashi, R.; Normand, J.; Raghavachari, K.; Rendell, A.; Burant, J. C.; Iyengar, S. S.; Tomasi, J.; Cossi, M.; Rega, N.; Millam, J. M.; Klene, M.; Knox, J. E.; Cross, J. B.; Bakken, V.; Adamo, C.; Jaramillo, J.; Gomperts, R.; Stratmann, R. E.; Yazyev, O.; Austin, A. J.; Cammi, R.; Pomelli, C.; Ochterski, J. W.; Martin, R. L.; Morokuma, K.; Zakrzewski, V. G.; Voth, G. A.; Salvador, P.; Dannenberg, J. J.; Dapprich, S.; Daniels, A. D.; Farkas, O.; Foresman, J. B.; Ortiz, J. V.; Cioslowski, J.; Fox, D. J. S. *Gaussian 09, Revision D.01*, Gaussian Inc.: Wallingford CT, 2009.
75. Hase, W. L.; Buckowski, D. G. Monte-Carlo Sampling of A Micro-Canonical Ensemble of Classical Harmonic-Oscillators. *Chemical Physics Letters* **1980**, *74* (2), 284-287.
76. Hase, W. L.; Duchovic, R. J.; Hu, X.; Komornicki, A.; Lim, K. F.; Lu, D.-H.; Peslherbe, G. H.; Swamy, K. N.; Vande Linde, S. R.; Zhu, L.; Varandas, A.; Wang, H.; Wolf, R. VENUS96: A general chemical dynamics computer program. *QCPE Bull.* **1996**, *16*, 43.
77. Stewart, J. J. P.; Fiedler, L. J.; Zhang, P.; Zheng, J.; Rossi, I.; Hu, W.-P.; Lynch, G. C.; Liu, Y.-P.; Chuang, Y. Y.; Pu, J.; Li, J.; Cramer, C. J.; Fast, P. L.; Truhlar, D. G. *MOPAC 5.022mn.*, Department of Chemistry and Supercomputing Institute, University of Minnesota, Minneapolis; Department of Chemistry and Supercomputing Institute, University of Minnesota, Minneapolis, 2015.
78. Rocha, G. B.; Freire, R. O.; Simas, A. M.; Stewart, J. J. P. RM1: A reparameterization of AM1 for H, C, N, O, P, S, F, Cl, Br, and I. *Journal of Computational Chemistry* **2006**, *27* (10), 1101-1111.
79. Spezia, R.; Martin-Somer, A.; Macaluso, V.; Homayoon, Z.; Pratihar, S.; Hase, W. L. Unimolecular dissociation of peptides: statistical vs. non-statistical fragmentation mechanisms and time scales. *Faraday Discussions* **2016**, *195*, 599-618.
80. Carra, A.; Spezia, R. In Silico Tandem Mass Spectrometer: an Analytical and Fundamental Tool. *Chemistry -Methods* **2021**, *1*, 123-130.
81. Martin-Somer, A.; Martens, J.; Grzetic, J.; Hase, W. L.; Oomens, J.; Spezia, R. Unimolecular Fragmentation of Deprotonated Diproline Pro(2)-H (-) Studied by Chemical Dynamics Simulations and IRMPD Spectroscopy. *Journal of Physical Chemistry A* **2018**, *122* (10), 2612-2625.
82. Citir, M.; Hinton, C. S.; Oomens, J.; Steill, J. D.; Armentrout, P. B. Infrared multiple photon dissociation spectroscopy of protonated histidine and 4-phenyl imidazole. *International Journal of Mass Spectrometry* **2012**, *330*, 6-15.
83. Hirata, K.; Mori, Y.; Ishiuchi, S.-I.; Fujii, M.; Zehnacker, A. Chiral discrimination between tyrosine and beta-cyclodextrin revealed by cryogenic ion trap infrared spectroscopy. *Physical chemistry chemical physics : PCCP* **2020**, *22* (43), 24887-24894.
84. Voronina, L.; Rizzo, T. R. Spectroscopic studies of kinetically trapped conformations in the gas phase: the case of triply protonated bradykinin. *Physical Chemistry Chemical Physics* **2015**, *17*, 25828-25836.

85. Sen, A.; Le Barbu-Debus, K.; Scuderi, D.; Zehnacker-Rentien, A. Mass Spectrometry Study and Infrared Spectroscopy of the Complex Between Camphor and the Two Enantiomers of Protonated Alanine: The Role of Higher-Energy Conformers in the Enantioselectivity of the Dissociation Rate Constants. *Chirality* **2013**, *25* (8), 436-443.
86. Bratakos, S. M.; Sinanoglou, V. J.; Matsoukas, M. T.; Siapi, E.; Papahatjis, D. P.; Riganakos, K.; Zoumpoulakis, P. Fragmentation Patterns of Aromatic 2,5-diketopiperazines Using Liquid chromatography/Mass Spectrometry. *Current Analytical Chemistry* **2016**, *12* (5), 439-449.
87. Chen, Y. H.; Liou, S. E.; Chen, C. C. Two-step mass spectrometric approach for the identification of diketopiperazines in chicken essence. *European Food Research and Technology* **2004**, *218* (6), 589-597.
88. Vandergreef, J.; Tas, A. C.; Nijssen, L. M.; Jetten, J.; Hohn, M. Identification and Quantitation of Diketopiperazines by Liquid-Chromatography Mass-Spectrometry, Using a Moving Belt Interface. *Journal of Chromatography* **1987**, *394* (1), 77-88.
89. Somogyi, A.; Wysocki, V. H.; Mayer, I. The Effect of Protonation Site on Bond Strengths in Simple Peptides - Application of Ab-Initio and Modified Neglect of Differential-Overlap Bond Orders and Modified Neglect of Differential-Overlap Energy Partitioning. *J. Am. Soc. Mass Spectrom.* **1994**, *5* (8), 704-717.

Table 1: Relative energies and relevant structural parameters for the most stable conformers of *c*-LLH⁺ and *c*-LDH⁺. The zero of the energy scale is taken at the most stable conformer for each diastereomer. *The most stable *c*-LDH⁺ conformer is 0.67 kcal/mol higher in energy than the most stable *c*-LLH⁺ conformer.

Structure	Interaction	Gibbs Free Energy ΔG (kcal/mol)	$\tau_1(^{\circ})$	$\tau_2(^{\circ})$	Distance between the centres of the aromatic rings (\AA)	NH ⁺ ...O distance (\AA)	CH... π distance (\AA)	NH... π distance (\AA)
$g_L^+t_D$	NH ⁺ ...O/CH... π	0 *	62	159	5.44	1.62	2.56 (C_{α})	...
$g_L^-t_D$	NH ⁺ ...O/NH... π	1.35	-58	155	9.16	1.59	...	3.20
$g_L^+t_L$	NH ⁺ ...O/CH... π	0	63	- 155	5.41	1.61	2.42(C_{β})	...
$g_L^-t_L$	NH ⁺ ...O/NH... π	2.23	-58	-57	9.10	1.61	...	3.18

Table 2: Assignment of the mass-to-charge peaks observed in the experimental MS² spectrum based on chemical dynamics simulations. The most abundant fragments are highlighted to facilitate comparison with the mass spectrum shown in Figure 4.

Experimental <i>m/z</i>	Molecular formula of the ionic fragment	Molecular formula of the neutral fragment	Reaction energy (kcal/mol)
	C ₁₅ H ₁₇ N ₄ O ₂ ⁺		
268.1	C ₁₅ H ₁₄ N ₃ O ₂ ⁺	NH ₃	42.9
267.1	C ₁₅ H ₁₅ N ₄ O ⁺	H ₂ O	39.9
257.1	C ₁₄ H ₁₇ N ₄ O ⁺	CO	41.1
240.1	C ₁₄ H ₁₄ N ₃ O ₁ ⁺	CH ₃ NO	73.1
		CO NH ₃	46.4
		CHN H ₂ O	71.1
239.1	C ₁₄ H ₁₅ N ₄ ⁺	CO H ₂ O	75.3
224.1	C ₁₄ H ₁₄ N ₃ ⁺	CHNO H ₂ O	71.4
222.1	C ₁₄ H ₁₂ N ₃ ⁺	CO H ₂ O NH ₃	115.4
212.1	C ₁₃ H ₁₄ N ₃ ⁺	CH ₃ NO CO	96.8
		CO CO NH ₃	70.1
207.1	C ₉ H ₁₁ N ₄ O ₂ ⁺	C ₆ H ₆	30.1
205.1	C ₁₁ H ₁₃ N ₂ O ₂ ⁺	C ₄ H ₄ N ₂	102.3
		C ₃ H ₃ N CHN	183.8
204.1	C ₁₁ H ₁₂ N ₂ O ₂ ⁺ [2]	C ₄ H ₅ N ₂ [2]	84.1
203.1	C ₁₁ H ₁₁ N ₂ O ₂ ⁺	C ₄ H ₆ N ₂	109.4
		C ₃ H ₅ N CHN	123.0
195.1	C ₈ H ₁₁ N ₄ O ₂ ⁺	C ₇ H ₆	98.5
194.1	C ₈ H ₁₀ N ₄ O ₂ ⁺ [2]	C ₇ H ₇ [2]	66.1
193.1	C ₈ H ₉ N ₄ O ₂ ⁺	C ₇ H ₈	64.4
189.1	C ₁₁ H ₁₃ N ₂ O ₁ ⁺	C ₃ H ₄ N ₂ CO	76.3
185.1	C ₁₂ H ₁₃ N ₂ ⁺	CH ₄ N ₂ CO CO	122.2
175.1	C ₁₀ H ₁₁ N ₂ O ⁺	C ₄ H ₆ N ₂ CO	125.0
168.1	C ₇ H ₁₀ N ₃ O ₂ ⁺	C ₈ H ₇ N	40.0
166.1	C ₇ H ₈ O ₂ N ₃ ⁺	C ₈ H ₉ N	117.4
		C ₇ H ₈ CHN	168.3
164.0	C ₇ H ₆ N ₃ O ₂ ⁺	C ₈ H ₉ N H ₂	91.5
160.1	C ₁₀ H ₁₀ NO ⁺	C ₃ H ₇ N ₃ O ₁	125.2
153.1	C ₆ H ₉ N ₄ O ₁ ⁺	C ₉ H ₈ O	70.7

138.1	$C_6H_8N_3O_1^+$	C_9H_9NO			92.5
		C_8H_9N	CO		62.5
		C_8H_7N	CH ₂ O		121.6
		C_7H_8	CO	CHN	113.4
133.1	$C_9H_9O^+$	$C_5H_7N_3$	CHNO		91.5
		$C_5H_5N_3$	CH ₃ NO		122.8
130.1	$C_9H_8N^+$	$C_5H_7N_3$	CO	H ₂ O	160.3
		$C_5H_6N_2O$	CH ₃ NO		260.5
123.1	$C_6H_7N_2O^+$	$C_9H_{10}N_2O$			56.8
		C_8H_9N	CHNO		69.4
		C_7H_8	CH ₂ N ₂	CO	112.9
		C_8H_7N	CO	NH ₃	74.0
121.0	$C_6H_5N_2O_1^+$	$C_9H_{12}N_2O$			55.7
		C_8H_9N	CH ₃ NO		114.2
		C_7H_8	C ₂ H ₄ N ₂ O		102.7
		C_8H_9N	CO	NH ₃	87.5
120.1	$C_8H_{10}N^+$	$C_7H_7N_3O_2$			115.7
		$C_6H_7N_3O$	CO		115.7
		$C_6H_4N_2O$	CH ₃ NO		130.0
		$C_4H_3NO_2$	C ₃ H ₄ N ₂		130.0
		$C_6H_4N_2O$	CO	NH ₃	103.4
		$C_5H_7N_3$	CO	CO	83.8
110.1	$C_5H_8N_3^+$	$C_{10}H_9NO_2$			108.5
		$C_{10}H_7NO$	H ₂ O		96.7
		C_9H_9NO	CO		101.5
		C_9H_8O	CHNO		61.2
		C_9H_6O	CH ₃ NO		115.6
		C_8H_9N	CO	CO	71.6
		C_8H_7N	CH ₂ O	CO	130.6
44.0	CH_2NO^+	$C_5H_7N_3$	C_8H_8	CO	126.3

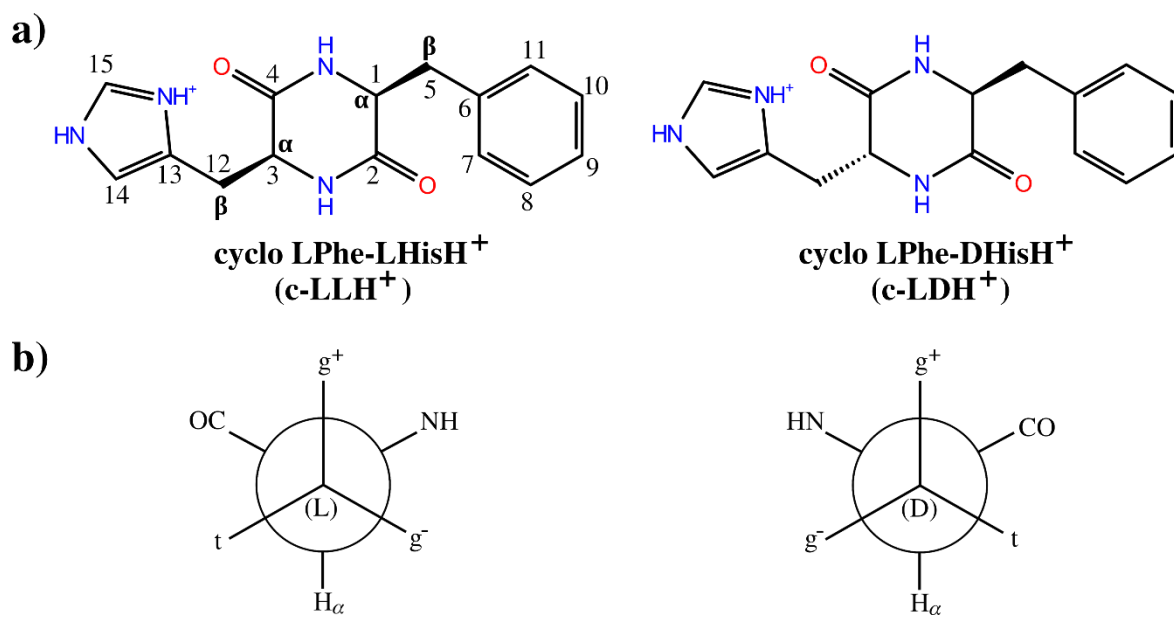


Figure 1: a) cyclo His-PheH⁺ with atom labeling. The angles used in the description of the aromatic substituents orientation are $\tau_1(\text{NC}_1\text{C}_5\text{C}_6)$ and $\tau_2(\text{NC}_3\text{C}_{12}\text{C}_{13})$. b) Newman projection showing the orientation of the substituents (see text).

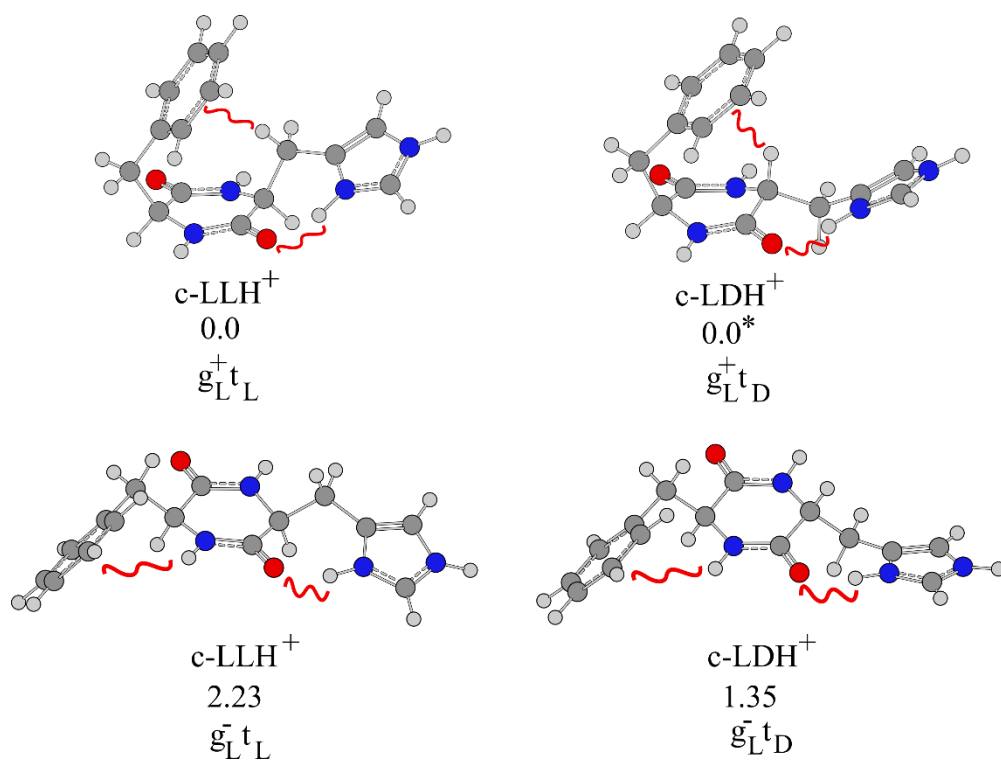


Figure 2 : Most stable structures of $c\text{-LLH}^+$ and $c\text{-LDH}^+$, with their relative Gibbs energies at room temperature. The curly red line highlights the interactions that stabilize the structures. The gray, light gray, blue and red color circles correspond to carbon, hydrogen, nitrogen and oxygen atoms, respectively. The zero of the energies is taken, for each diastereomer, at the most stable conformer. *The most stable $c\text{-LDH}^+$ conformer is higher in energy than the most stable $c\text{-LLH}^+$ conformer by 0.67 kcal/mol.

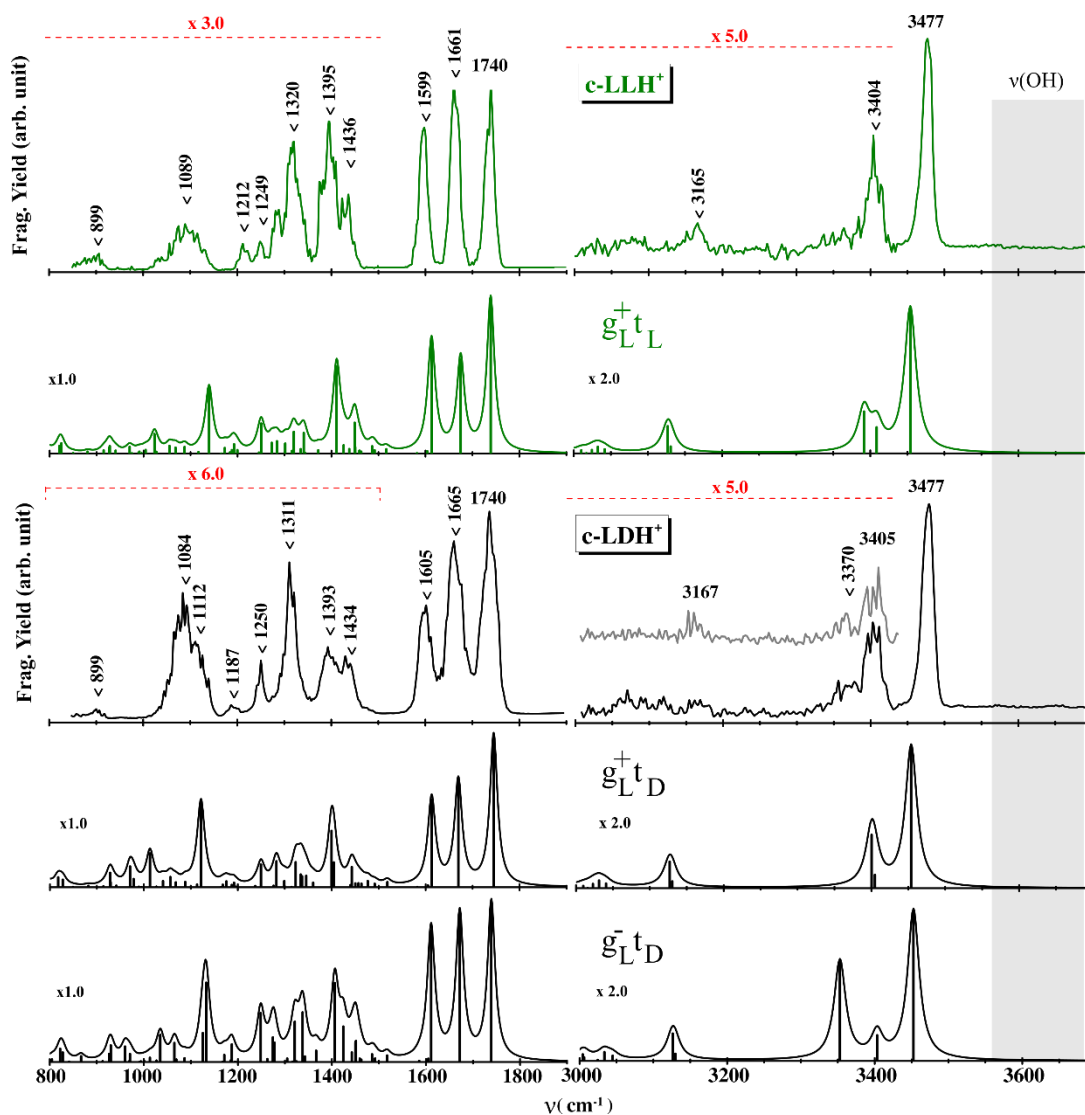


Figure 3: Comparison between the experimental IRMPD spectra (top spectrum) of both diastereomers and the simulated IR absorption spectrum of the most stable structures to which the experimental spectra are assigned (see Figure 2). The y-axis (fragmentation yield and IR absorption) is in arbitrary unit. The simulated IR spectra are obtained by convoluting the harmonic frequencies (stick bars) with a Lorentzian line shape of 10 cm^{-1} FWHM. The OH stretch region is highlighted in light grey.

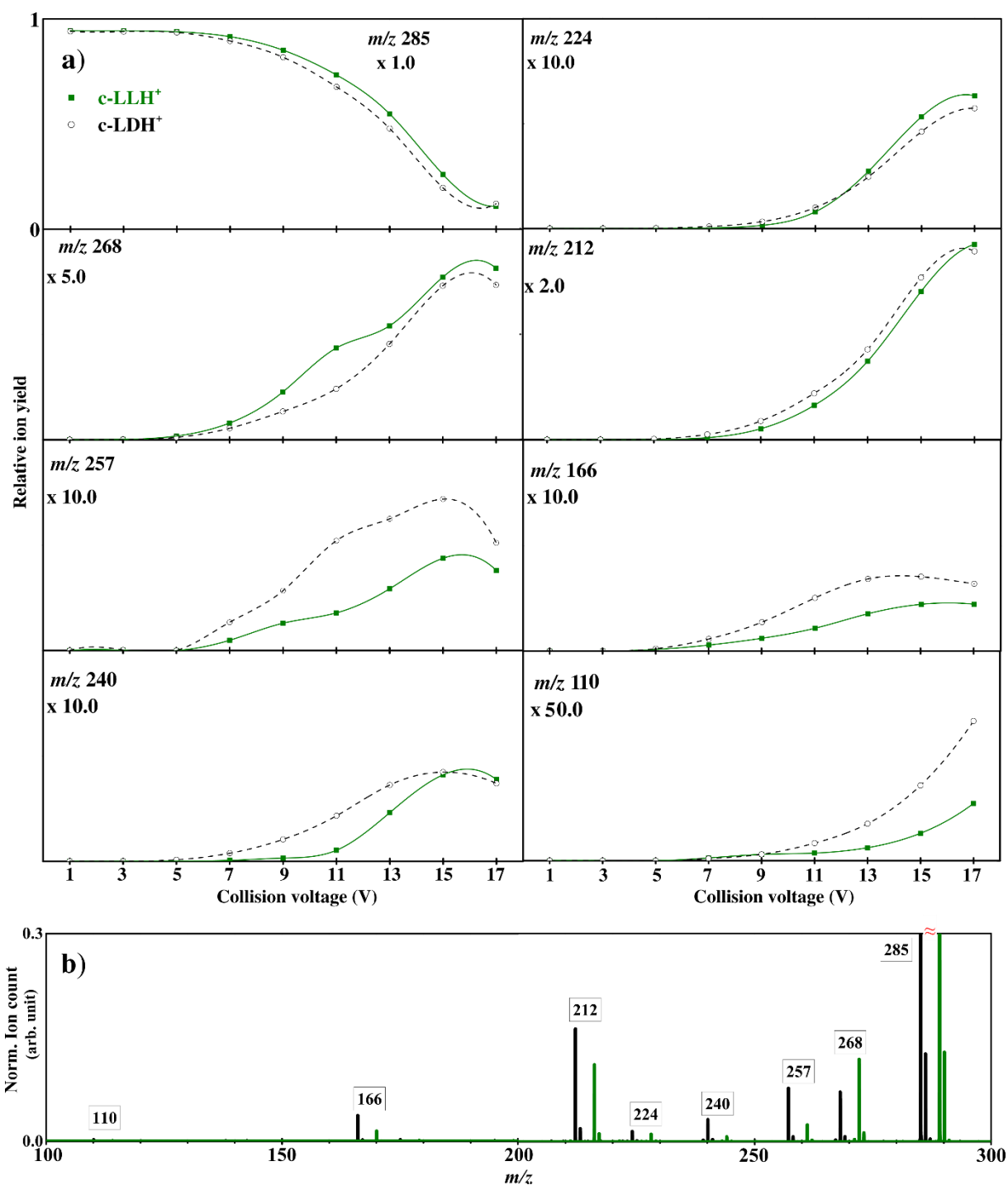
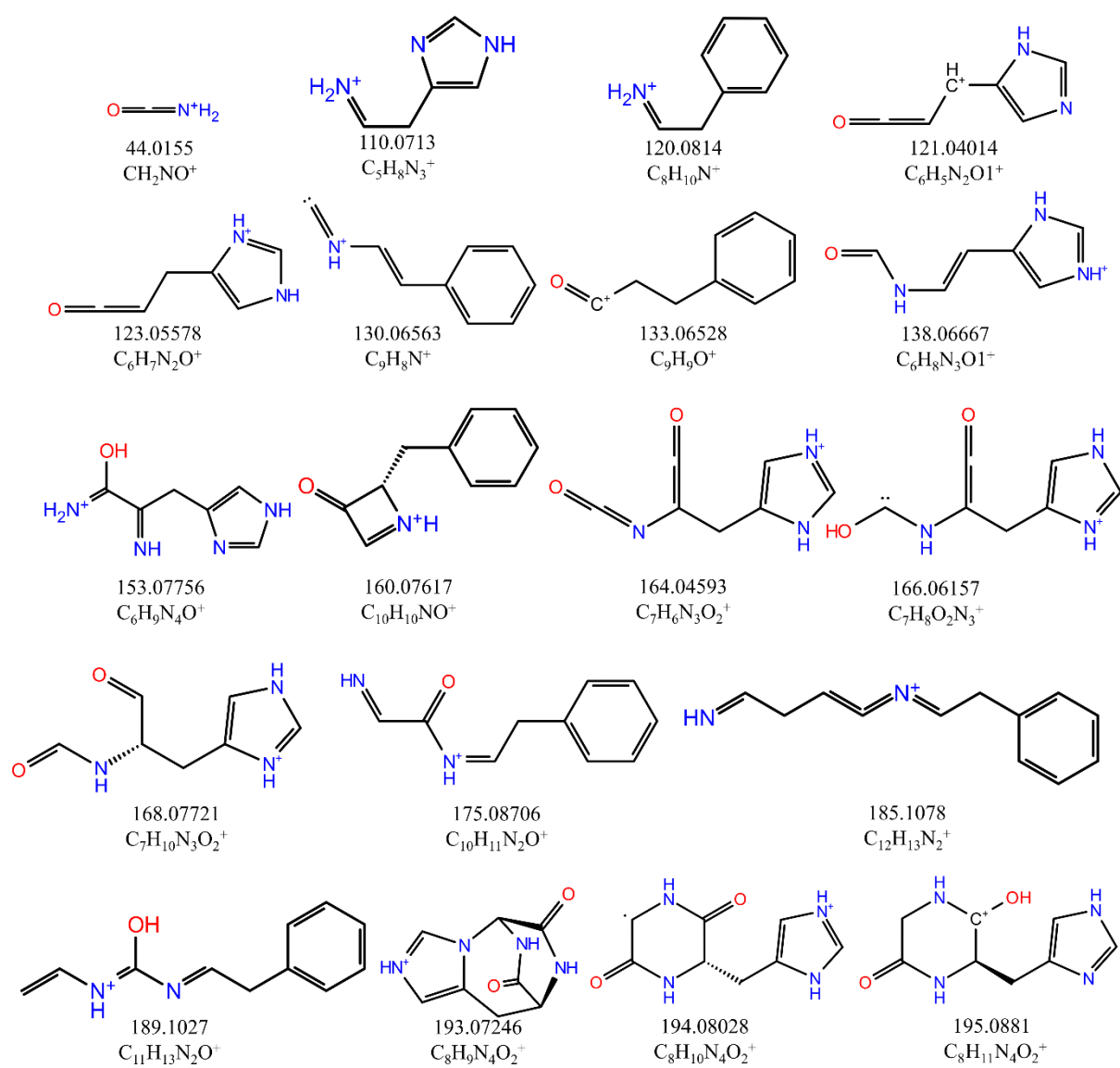


Figure 4 CID-MS² analysis for the two diastereoisomers. a) Total fragmentation efficiency and relative ion yield (branching ratio) per m/z channels as a function of the collision voltage for c-LLH⁺ (green, squares with full line) and c-LDH⁺ (black, empty circles with dashed line). The vertical scale is from 0 to 1 and the "x n" factor indicated at the top left of each graph indicates the multiplication factor relative to m/z 285. Dashed and continuous lines are a guide for the eyes. b) CID-MS² spectrum of c-LLH⁺ (green) and c-LDH⁺ (black) at 11 V. The intensities are normalized at the intensity of the parent ion for a direct comparison. The c-LLH⁺ spectrum is shifted up by 4 amu for the sake of clarity.



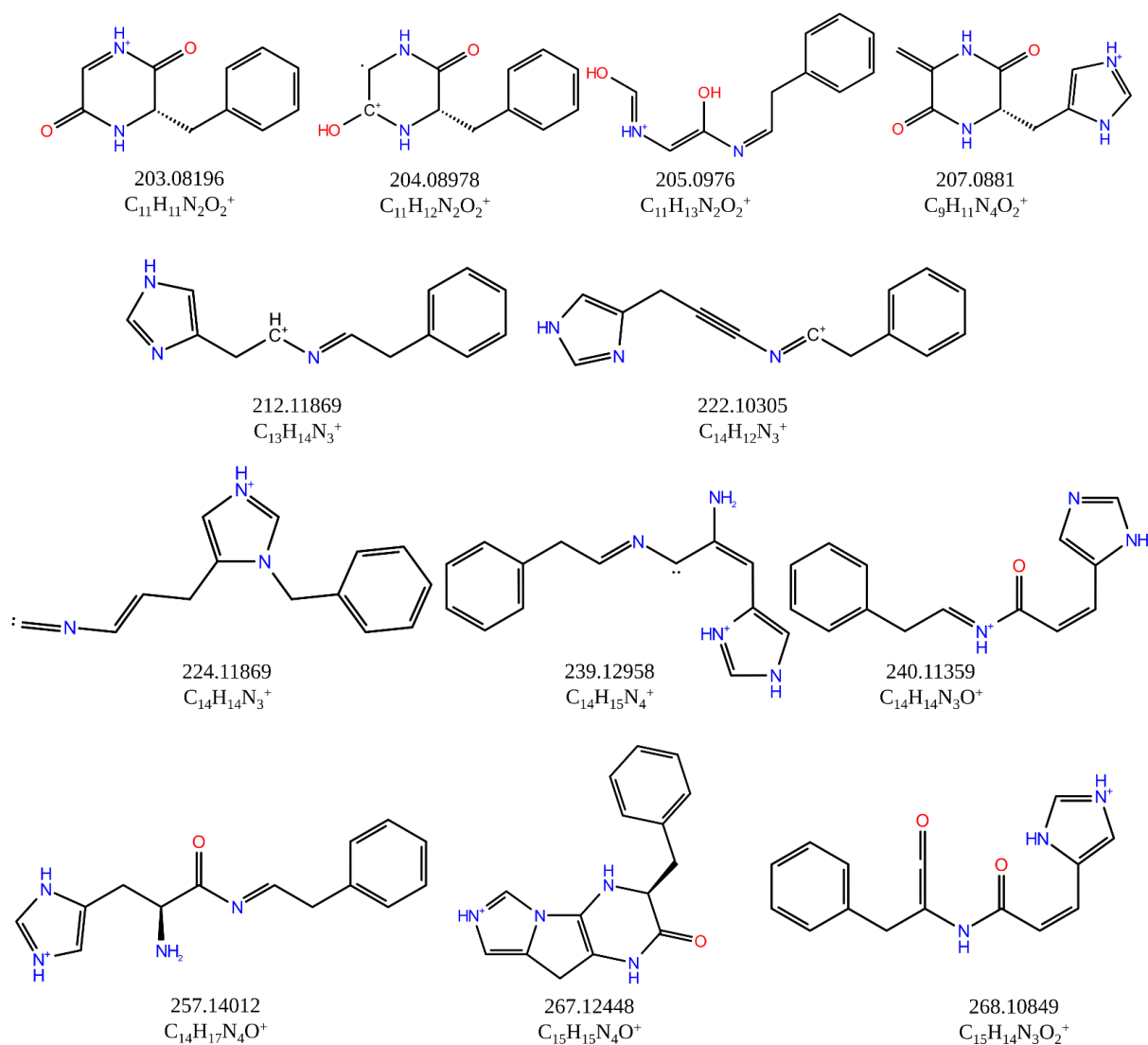


Figure 5: The most abundant isomers for each m/z fragment produced by CID and their molecular formula as obtained from chemical dynamics simulations.

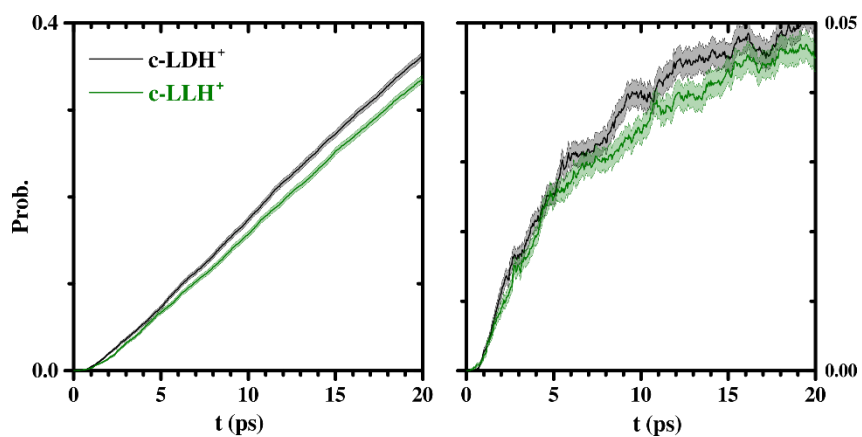


Figure 6 : Diastereomeric comparison based on chemical dynamic simulation at 517 kcal/mol: (left) total fragmentation yield as a function of time. (right) formation yield of m/z 257 as a function of propagation time. The shaded areas represent the uncertainty.

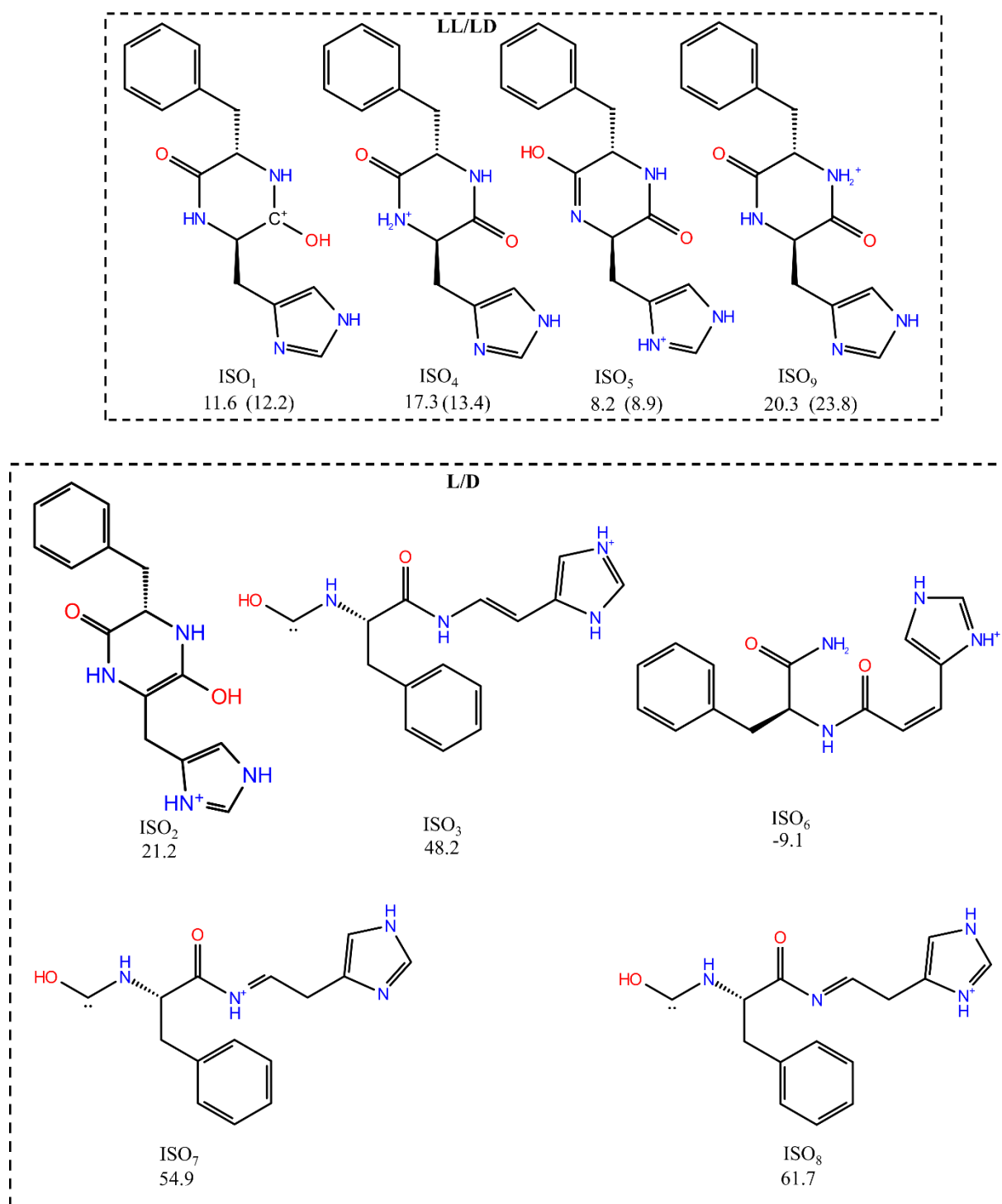


Figure 7 The main intermediate isomers as obtained from the chemical dynamic simulations. They are grouped according to the number of chiral centers they contain. Their relative energy after optimization at the DFT level are given for each isomer in kcal/mol. For those containing two stereogenic centers, the first energy value corresponds to LL and the value in parentheses to LD.

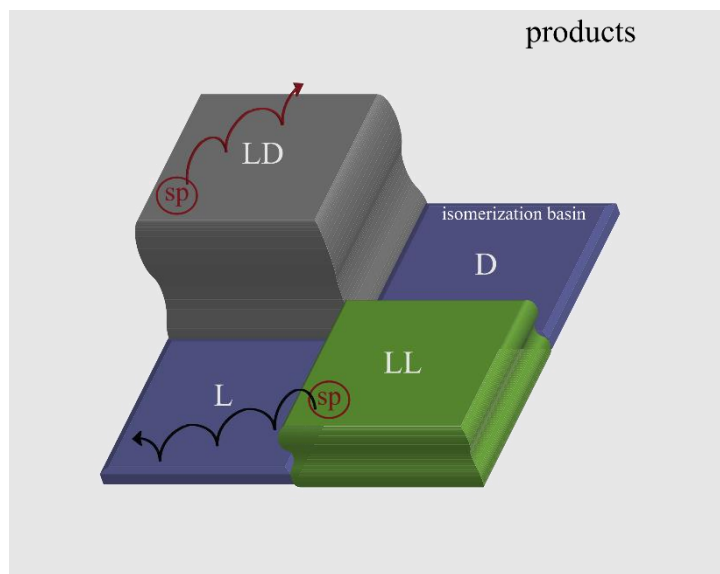


Figure 8: Schematic view of the diastereoselective CID mechanism. The sketch shows how isomeric forms of the fragmentation intermediate are sensitive to stereochemical factors (LL vs. LD) or not (L vs. D). The vertical axis corresponds to the relative energy of the potential-energy surface regions. The outer region of the sketch corresponds to the products. “sp” stands for starting point referring to the activated reagent geometry.

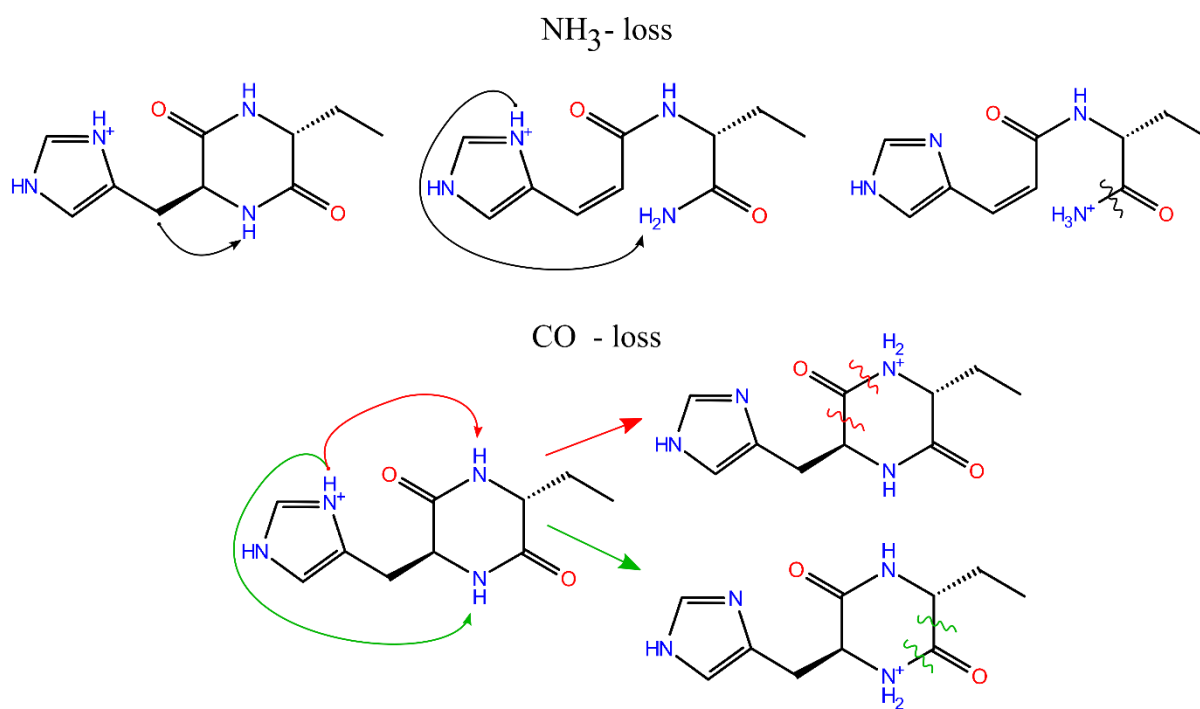


Figure 9: Sketch of the reaction leading to NH₃ loss (top) and involving Group 2 (predissociated) intermediate states. Sketch of the reaction resulting in CO loss (bottom) and involving Group 1 (non predissociated, *i.e.* cyclic) intermediate states. The red and green arrows indicate the two possible CO loss processes from the two residues.

Structure and Collision-Induced Dissociation of the protonated cyclo His-Phe Dipeptide: Mechanistic Studies and Stereochemical Effects.

Ariel Pérez-Mellor,^{a)b)} Katia Le Barbu-Debus,^{a)} Valeria Lepere,^{a)} Ivan Alata,^{a)} Riccardo Spezia^{b)} Anne Zehnacker,^{a)}*

a) Université Paris-Saclay, CNRS, Institut des Sciences Moléculaires d'Orsay, 91405, Orsay, France

b) Laboratoire de Chimie Théorique, Sorbonne Université, UMR 7616 CNRS, 4, Place Jussieu, 75005 Paris, France.

* anne.zehnacker-rentien@universite-paris-saclay.fr

Supplementary Information

Table S1: Assignment of the experimental frequencies to the calculated ones, together with mode description for c-LLH⁺. The calculated frequencies are scaled by 0.97 in the 800-2000 cm⁻¹ region and 0.955 in the 3000-3800 cm⁻¹ range

c-LLH ⁺		
Experimental frequencies	Calculated values	
	g [†]	
	Harmonic frequencies in cm ⁻¹ (intensity in km/mole)	Mode
3477	3454 (191)	Free v(NH) _{Imidazole}
3404	3409 (34)	Free v(NH) _{DKP} on the free amide
	3391 (55)	Free v(NH) _{DKP} on the H-bond accepting amide
3165	3131 (9)	Symmetric v(CH) _{Imidazole}
	3127 (36)	Asymmetric v(CH) _{Imidazole}
-	2752 (1311)	Bound v(NH ⁺) _{Imidazole}
1740	1739 (410)	v(CO)
1661	1675 (248)	v(CO)
1599	1613 (298)	v(CC)
1436	1449 (81)	β(C _β H ₂) bend on Phe
1395	1411 (231)	β(C _β H ₂) bend on His
1320	1139 (174)	Delocalized motions
1249		
1212		
1089		

Table S2: Assignment of the experimental frequencies to the calculated ones, together with mode description for c-LDH⁺. The calculated frequencies are scaled by 0.97 in the 800-2000 cm⁻¹ region and 0.955 in the 3000-3800 cm⁻¹ range

c-LDH ⁺				
Experimental frequencies	Calculated values			
	g ⁺ t		g ⁻ t	
	Harmonic frequencies in cm ⁻¹ (intensity in km/mole)	Mode	Harmonic frequencies in cm ⁻¹ (intensity in km/mole)	Mode
3477	3454 (187)	Free v(NH) _{Imidazole}	3453 (199)	Free v(NH) _{Imidazole}
3405	3405 (17)	Free v(NH) _{DKP} on the free amide	3403 (34)	Free v(NH) _{DKP}
	3400 (70)	Free v(NH) _{DKP} on the H-bond accepting amide	-	-
3370		-	3353 (13136))	Bound v(NH) _{DKP} on the H-bond accepting amide
3167	3130 (9)	Symmetric v(CH) _{Imidazole}	3130 (9)	Symmetric v(CH) _{Imidazole}
	3127 (35)	Asymmetric v(CH) _{Imidazole}	3126 (36)	Asymmetric v(CH) _{Imidazole}
-	3818 (1237)	Bound v(NH ⁺) _{Imidazole}	2717 (1780)	Bound v(NH ⁺) _{Imidazole}
1740	1745 (402)	v(CO)	1739 (420)	v(CO)
1665	1670 (279)	v(CO)	1672 (388)	v(CO)
1605	1613 (231)	v(CC)	1611 (346)	v(CC)
1434	1443	β(C _β H ₂) bend on Phe	1451 (55) 1450 (50) 1424 (93)	Delocalized β(NH) and β(CH)
			1406 (208)	Bound β(NH)
1393	1404 (65) 1400 (149)	β(C _β H ₂) bend on His	-	-
1311-1112	1346 (30)	Delocalized motions	1338 (131)	Delocalized motions
	1334 (66)		1321 (106)	
	1323 (33)		1278 (51)	
	1282 (68)		1274 (65)	
	1249 (60) 1176 (15)		1248 (129) 1187 (46)	
1112	1122 (223)	β(CH) _{Imidazole}	1133 (209)	β(CH) _{Imidazole}

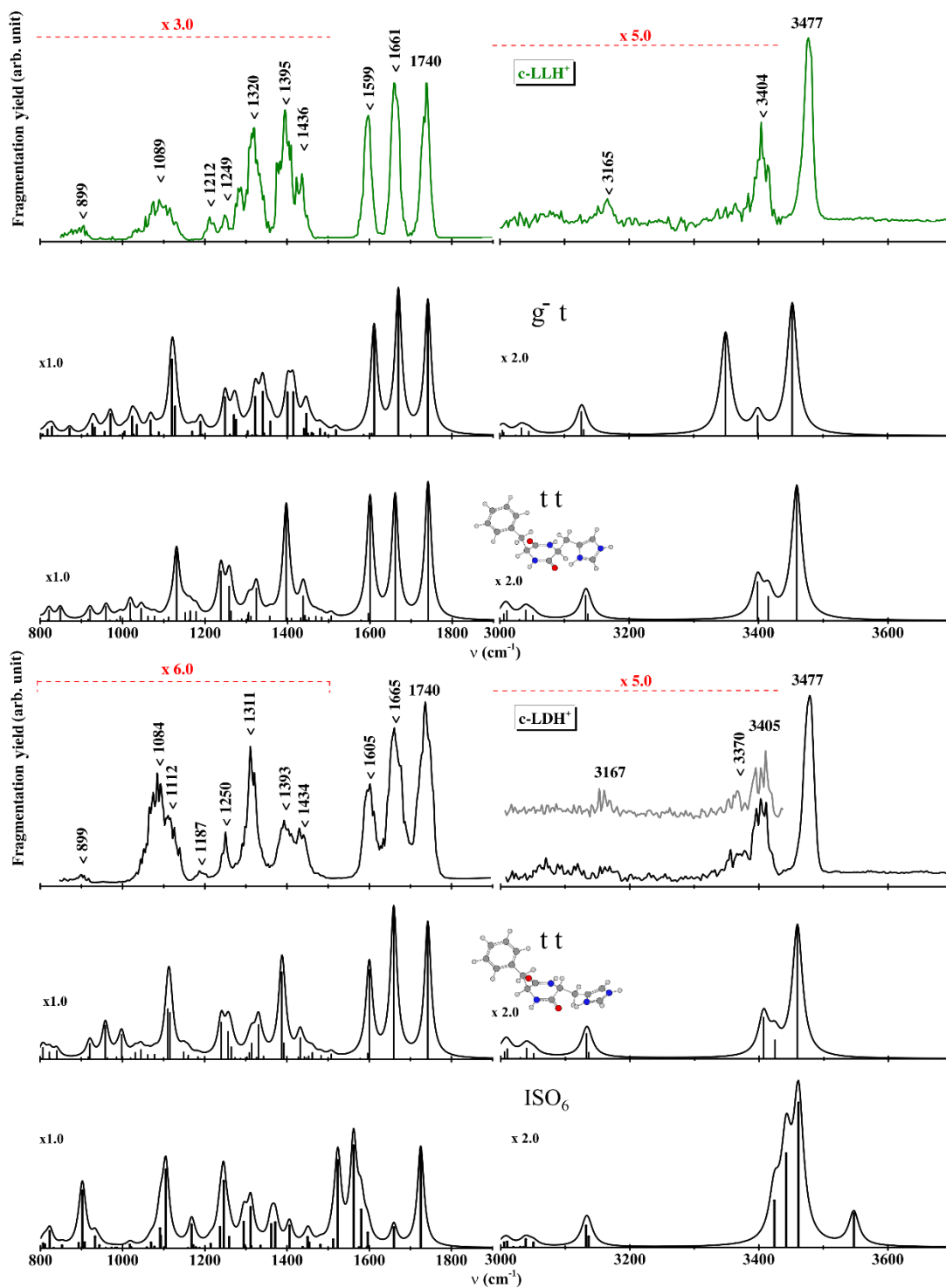
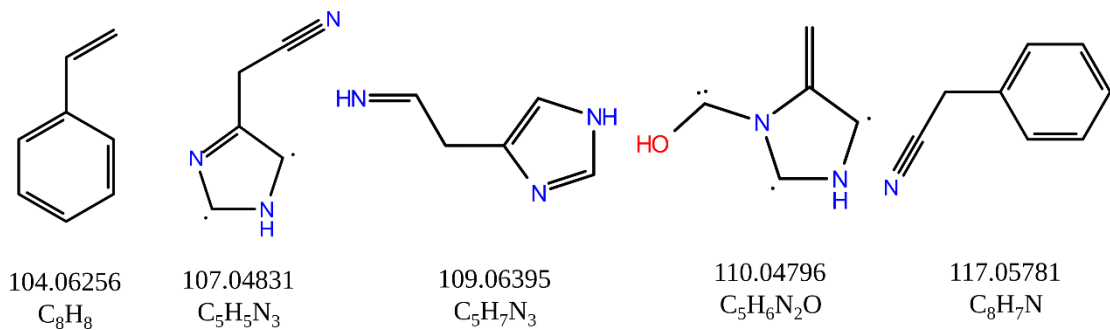
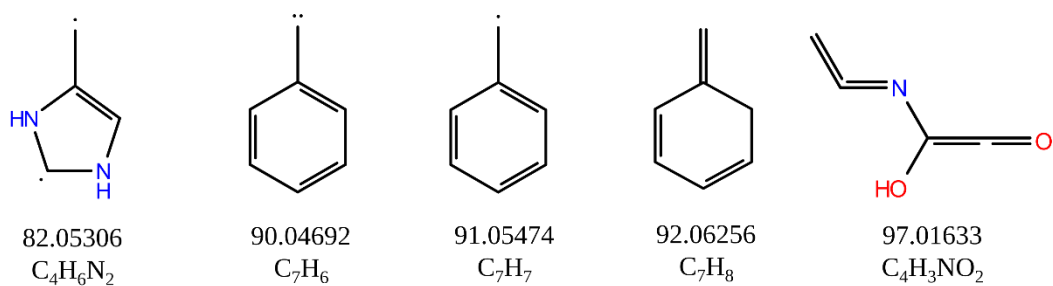
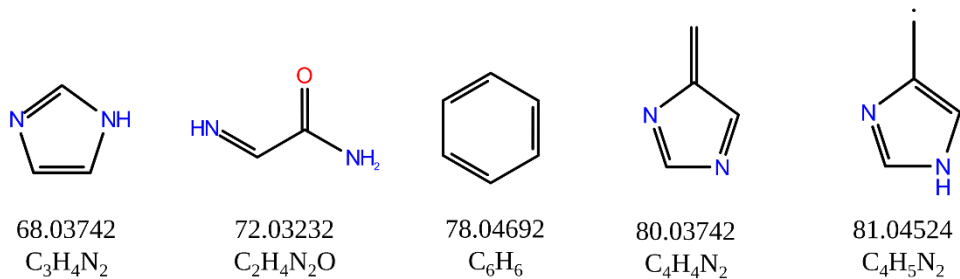
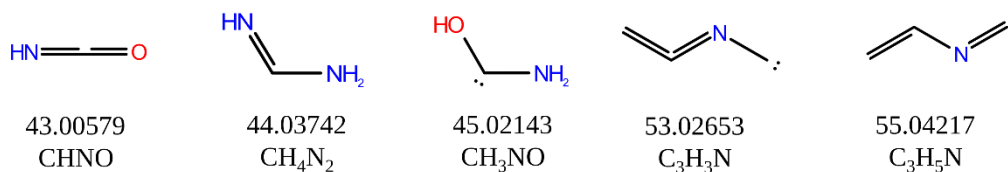


Figure S1: Experimental spectrum of c-LLH⁺ and c-LDH⁺ compared to calculated structures not retained for the assignment.

HH	NH ₃	H ₂ O	:≡NH	:≡O	:—OH	N≡—NH ₂
2.01564	17.02653	18.01054	27.01089	27.9949	30.01054	42.02178
H ₂	NH ₃	H ₂ O	HCN	CO	CH ₂ O	CH ₂ N ₂



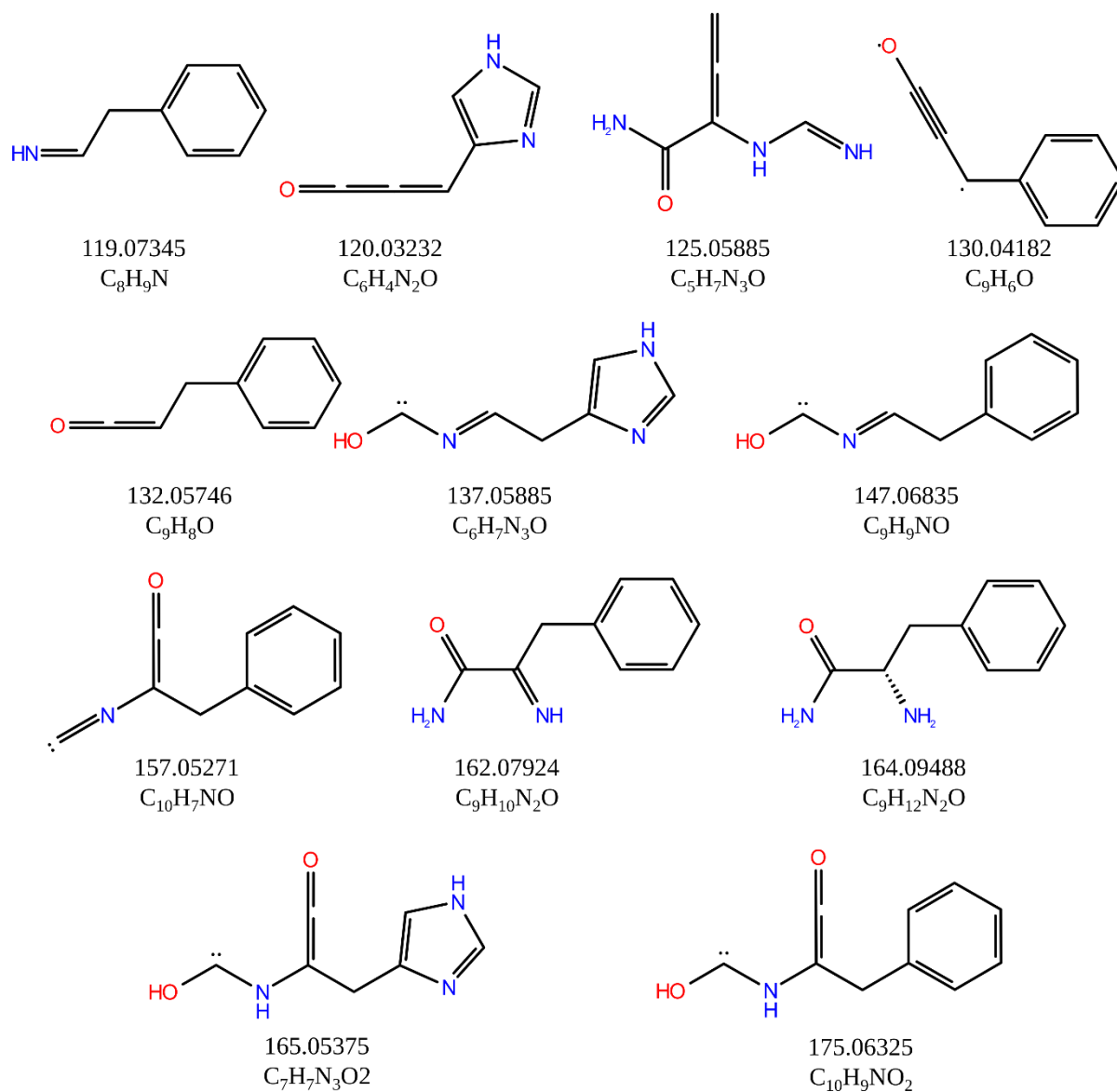


Figure S2: The most abundant isomers of the neutral fragment and their molecular formula as obtained from chemical dynamics simulations.

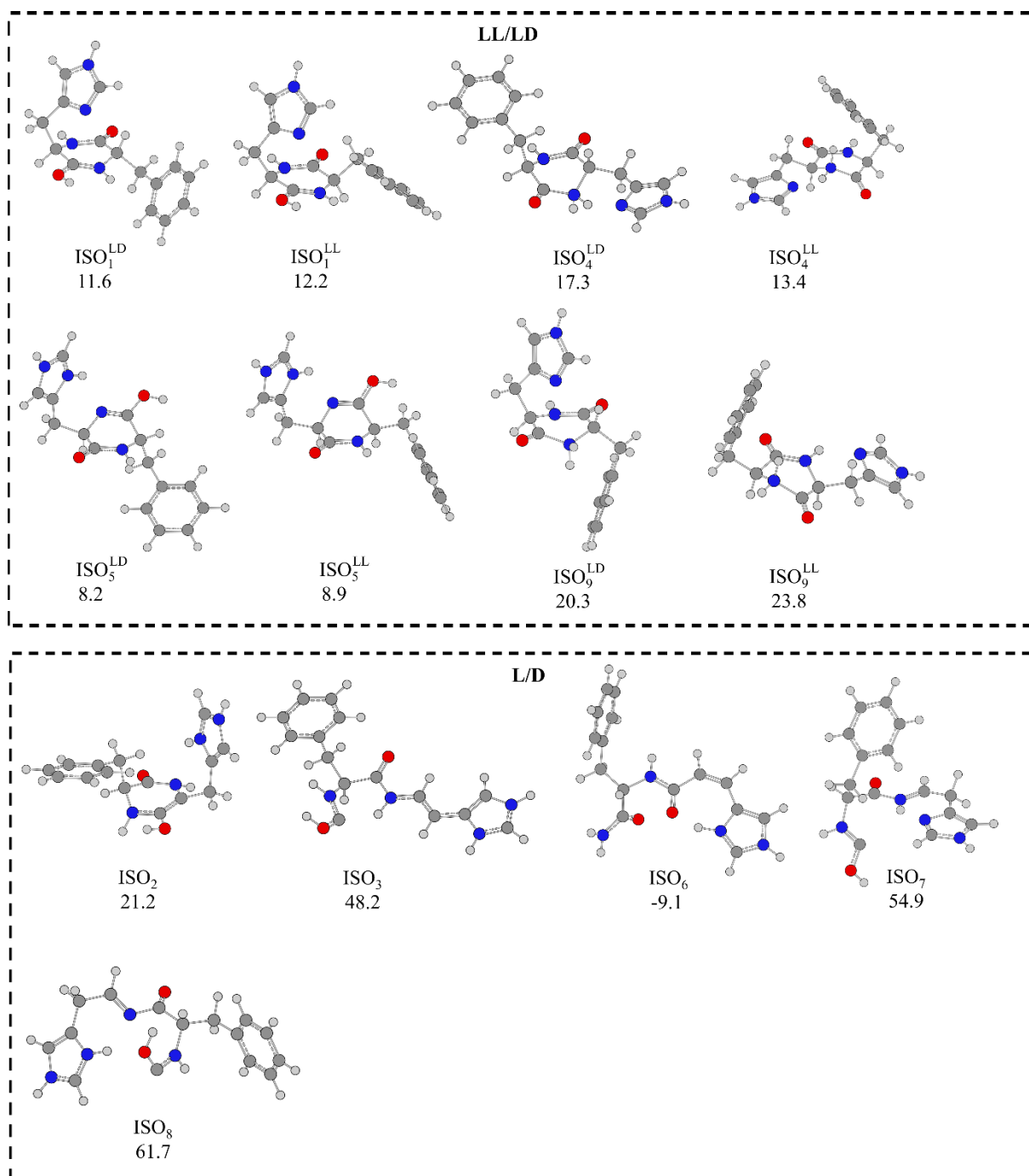


Figure S3: Comparison between the most abundant intermediate isomers for LL⁺ and LDH⁺.